8-3-2017

Impacts of De-icing Salt Contamination of Groundwater in a Shallow Urban Aquifer

Lukas McNaboe
luke.mcnaboe@gmail.com

Impacts of De-icing Salt Contamination of Groundwater in a Shallow Urban Aquifer

---

Lukas Adam McNaboe

B.S. University of Connecticut, 2015

A Thesis

Submitted in Partial Fulfillment of the

Requirements for the Degree of

Master of Science

At the

University of Connecticut

2017

Approval Page

Master of Science Thesis

Impacts of De-icing Salt Contamination of Groundwater in a Shallow Urban Aquifer

Presented by

Lukas A. McNaboe, B.S.

Major Advisor

Michael E. Dietz

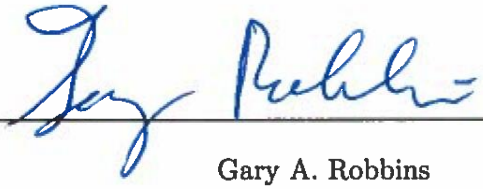

Associate Advisor

Gary A. Robbins

Associate Advisor

Timothy M. Vadas

University of Connecticut

2017

Acknowledgements

Perhaps to the physicist's dismay, research is not conducted in a vacuum. Similarly, this thesis would not exist without the insight, guidance, and support that so many people shared with me during this process.

I would like to acknowledge my advisor Dr. Michael Dietz, for his mentorship and friendship, for setting expectations that allowed me to grow as a professional researcher, and for holding me to a gold standard of quality in my work and at home. The value I place on Dr. Dietz's trust and patience is incalculable. I would also like to acknowledge Dr. Gary Robbins for providing a relentless stream of questions, books, and anecdotes that encouraged my creativity and other 'right-side brain-push-ups.' I'd like to thank Dr. Timothy Vadas for encouraging me to pursue graduate studies in the first place, for offering assistance with laboratory analysis, and for demonstrating the virtue of good listening.

I would like to thank Susan Isch and Paul Milne at the Connecticut Department of Public Health for assistance with sample analysis, much of this research would not have been possible without their time, interest, and generosity. I must acknowledge Gary Ulatowski and Chris Perkins at the Center for Environmental Science and Engineering for help with well drilling and installation. I'd like to thank Gary for being the physical embodiment of 'attention-to-detail' and for showing me the value of doing it the long way.

I must also thank my fellow graduate students for the network of accountability, afternoon frisbee sessions, lunch rides, and evening runs: all critical components of a successful workday. Lastly, I'd like to thank my family, friends and my girlfriend for their questions, support, and love through this journey. Thank you for making sure I knew the answer to that hardest question: *why?*

Contents

1 Literature Review **1**
- 1.1 Introduction . . . 1
- 1.2 Pervious pavement . . . 3
- 1.3 Winter de-icing . . . 6
  - 1.3.1 De-icing trends . . . 7
  - 1.3.2 Environmental transport and fate of de-icing salt . . . 8
  - 1.3.3 Ecological impacts . . . 10
- 1.4 Environmental radionuclides . . . 12
  - 1.4.1 A note on units . . . 12
  - 1.4.2 Radon . . . 13
  - 1.4.3 Radium . . . 16
- 1.5 Conclusion . . . 18

2 Thesis: Impacts of de-icing salt contamination of groundwater in a shallow urban aquifer **19**
- 2.1 Introduction . . . 19
- 2.2 Methods . . . 20
  - 2.2.1 Study site . . . 20
  - 2.2.2 Groundwater quality monitoring . . . 22
  - 2.2.3 Sampling and analysis . . . 23
  - 2.2.4 Equilibrium vapor-phase Rn calculations . . . 24
  - 2.2.5 Soil analysis . . . 24
- 2.3 Results and discussion . . . 25
  - 2.3.1 Summary of climatological observations . . . 25
  - 2.3.2 Soil analysis . . . 26
  - 2.3.3 Site water table elevation . . . 30
  - 2.3.4 Groundwater quality monitoring . . . 36
    - 2.3.4.1 Long-term monitoring: Chloride . . . 37
    - 2.3.4.2 Radionuclides . . . 46
    - 2.3.4.3 Metal cations . . . 51
    - 2.3.4.4 Vertical variation . . . 53
- 2.4 Conclusion . . . 54
- 2.5 References . . . 56

Appendices **62**

A Boring logs **63**

B Equilibrium vapor-phase Rn calculations **69**

C Statistical analysis **70**

D Chloride travel time calculations **76**

List of Figures

1.1 Cross section diagram of typical permeable pavement, showing upper infiltration layers and infiltrate reservoir. Native soil underlies this sub-base layer. 5
1.2 Annual road salt use in million metric tons is represented as black squares. Road salt use as a percentage of the total national salt consumption is represented as red circles. Data compiled from USGS mineral yearbooks, 1940-present. 6
1.3 Annual de-icing salt application as a function of total snowfall, broken up by pre- and post-implementation of anti-icing. Data from Mahoney et al. (2015). 7

2.1 Location of the study area within the Northeastern US (denoted by black star on left), and location of study site within UConn campus (circled on right). 21
2.2 Diagram of the study site, well locations are labeled and denoted by black circles. PZ represents a nest of 3 piezometers. 21
2.3 (Left) abridged description of soil core with soil color. (Right) down-core plot of soil Cl- content (mg/kg) from core sample taken at DG-4. 27
2.4 (Left) abridged description of soil core with color. (Right) down-core plot of soil Cl- content (mg/kg) from core sample taken at the prospective location of well UG-2, 50m south of (upgradient from) well UG-1. 28
2.5 Study site on the University of Connecticut campus in Storrs, CT. The red arrow shows direction of groundwater flow during dry periods. Contours show the elevation of the water table. Black labeled and numbered dots are shallow wells. PZ is a piezometer cluster. 30
2.6 Water table elevation (WTE) over time in well UG-1. 31
2.7 Water table elevation (WTE) over approximately 1.5 years in well DG-1. Gaps in the record are present when the sensor was removed for cleaning, had a dead battery, or during low-flow sampling. 31
2.8 Water table elevation (WTE) over approximately 2 years in well DG-2. Gaps in the record are present when the sensor was removed for cleaning, or during low-flow sampling. 33
2.9 Variation in water table elevation (WTE) over approximately 1 year in the shallow well of the nested piezometer (PZ-S). Gaps in the record are present when the sensor was removed for cleaning, or during low-flow sampling. . . . 33
2.10 Variation in water table elevation (WTE) over approximately 1 year at well DG-3. Gaps in the record are present when the sensor was removed for cleaning, or during low-flow sampling. 35

2.11 Water table elevation (WTE) over approximately 1 year at well DG-4. Gaps in the record are present when the sensor was removed for cleaning, or during low-flow sampling. 35
2.12 37
2.13 Cl^- concentration in well UG-1 during the period of study. Gaps in the record are present during probe failure, or when the probe was removed for cleaning or sampling. 39
2.14 Cl^- concentration in well DG-1 during the period of study. Gaps in the record are present during probe failure, or when the probe was removed for cleaning or sampling. 39
2.15 Cl^- concentration in well DG-2 during the period of study. Gaps in the record are present during probe failure, or when the probe was removed for cleaning or sampling. 41
2.16 Cl^- concentration in well PZ-S during the period of study. Gaps in the record are present during probe failure, or when the probe was removed for cleaning or sampling. 41
2.17 Cl^- concentration in well DG-3 during the period of study. Gaps in the record are present during probe failure, or when the probe was removed for cleaning or sampling. 43
2.18 Cl^- concentration in well DG-4 during the period of study. Gaps in the record are present during probe failure, or when the probe was removed for cleaning or sampling. 43
2.19 Box plots of all Cl^- data for each well. The median and mean Cl^- are represented by solid and dashed lines, respectively. The lower and upper black circles denote 5^{th} and 95^{th} percentiles. Wells with different letters are significantly different according to Tukey's HSD test, $\alpha = 0.05$. Mean separation was performed on a log-transformation of the data. Outliers are not plotted. 45
2.20 Box plots comparing Cl^- data from UG-1 with that of all other wells (DG-1 to 4, PZ-S). Means (dotted line) are significantly different based on a Satterthwaite 2-sample t-test ($p<0.0001$) 46
2.21 Spatial interpolations of (A) Na^+, (B) combined $^{226}Ra + ^{228}Ra$, and (C) ^{222}Rn. Concentration contours were generated in ArcMap using a natural neighbor algorithm. 47
2.22 Positive correlation ($p<0.001$) between Ra activity and Na^+ concentration for groundwater samples. 48
2.23 Negative exponential correlation ($p=0.054$) between aqueous Rn and conductivity (as a proxy for TDS), as described by eqn. 2.1. The Rn sample from well DG-4 was excluded from regression analysis. 49
2.24 Concentrations of major cations in groundwater samples for well DG-1. . . . 52
2.25 Molar comparison of Na^+ and Cl^- ions. Note that the slope of the linear regression is 0.72, indicating a deficiency of Na^+ relative to Cl^- 52
2.26 Spatial distributions of Mg^{2+} (left) and Ca^{2+} (right) dissolved ion concentrations in groundwater samples. Contour surfaces were generated using a natural neighbor interpolation algorithm. 53

Literature Review

1.1 Introduction

For decades, different strategies have been implemented to keep roadways safe and free from ice during winter months. Crystallized, wetted salt compounds (primarily sodium chloride (NaCl), although trace amounts of calcium and magnesium chloride ($CaCl_2$ and $MgCl_2$) are also used) are applied to roads before, during and after storm events in order to lower the freezing point of water, minimizing the formation of ice (Mullaney et al. 2009; Cassanelli and Robbins, 2013). Once this purpose has been realized, it is too late and impractical to clean de-icing agents from paved surfaces. Instead, these compounds are transported with melt water, where they either percolate to aquifers belowground, or run directly into surface water bodies.

In surface water systems, chloride (Cl^-) is chronically toxic to aquatic life at 230 mg L^{-1} and acutely toxic at 860 mg L^{-1} (US EPA, 1986). While long-term investigations of salt-affected streams and lakes document less than 150 mg L^{-1} Cl^- , (Corsi et al. 2015; Kelly et al. 2008; Kaushal, 2005) these studies identify gradual, steady increases in surface water Cl^- concentration over the past 30 years. Based on these trends, Corsi and others (2015) have noted that the chronic aquatic toxicity for Cl^- will be exceeded within the century.

Kaushal and others (2005) indicate a relationship between a stream's average Cl^- and that watershed's impervious cover fraction.

Regardless of a watershed's percent impervious cover (IC), de-icing salt applied to roads enters local waters by infiltration and as runoff. This presents many environmental problems. In many urban streams, Cl^- concentrations exceed chronic aquatic toxicity during winter months. During non-salting months (i.e. May through October), Cl^- is present at an increasing rate in baseflow, suggesting that groundwater discharge represents a long-term source of Cl^- to water bodies (Novotny et al. 2009). In groundwater systems, increased salt facilitates metal and cation mobility (Norrström and Jacks 1998; Bäckström et al 2004). This enhanced metal solvency in water due to dissolved Cl^- can also enhance corrosion of pipes (WHO 1978). Long-term ingestion of high levels of sodium (Na^+) exacerbates hypertension and heart disease, especially in children (WHO 1978). In a study of two neighboring communities of drinking water with Na^+ content of 8 and 108 mg L^{-1}, significantly higher blood pressure was found in the community of higher Na^+, when controlling for 18 other variables (Calabrese and Tuthill 1978). The overall World Health Organization (WHO) recommendation for Na^+ was to limit concentrations at lowest practicable levels, and to reduce Na^+ intake from other sources in areas where this is not possible. In addition to this inherent concern, the presence of radium in groundwater is largely controlled by that water's salinity (Kraemer and Reid 1984; Sturchio et al. 2001; Wood et al. 2004; Kumar et al. 2016). As the salinity of a groundwater system increases, gases such as dissolved radon will more readily partition to the gas phase, where it poses an inhalation hazard.

This literature review will discuss the practice of winter de-icing and the environmental impacts of this practice. Stormwater management systems will also be introduced as this study focuses on an area of pervious pavement. Additionally, the formation, transport, and fate of naturally-occurring radium and radon will be discussed to provide background information on these salinity-dependent elements.

1.2 Pervious pavement

One of the leading examples of nonpoint source pollution, urban stormwater runoff diminishes water quality in lakes, streams and estuaries (National Research Council, 2008). Higher streamflow following storms presents flooding and erosion problems; runoff can also carry fertilizers, oil, salt, heavy metals and other toxicants into waterways, further degrading aquatic ecosystems. While storms in forested watersheds can generate high streamflow, the erosion and contamination are not as pronounced due to their characteristically lower runoff coefficients (Chow et al. 1988). In more developed watersheds, this degradation is known as 'urban stream syndrome,' as urban watersheds are characterized by greater proportions of runoff than their less-developed counterparts (Walsh et al. 2005). Rural and forested watersheds tend to generate less surface runoff as a greater amount of precipitation has the opportunity to percolate through the soil; this subterranean flow path is much slower than paved surfaces, which directly channel runoff to waterways.

A watershed's propensity to generate stormwater runoff is commonly predicted by its percentage of impervious cover (IC), which consists of paved surfaces or highly compacted soil (Arnold and Gibbons, 1996). As mentioned previously, these surfaces act as conduits for runoff. In order to address this, these conduits can be circumvented with various green infrastructure systems. Pervious pavement is one such system; as its name suggests, this paved surface differs from its traditional counterparts in that precipitation can percolate through to the soil, reducing peak flows and runoff volume, and increasing lag time during storms (Dietz 2007; Hood et al. 2007). By implementing low-impact development (LID) practices such as permeable pavements, bioretention areas (e.g. rain gardens, bioswales), and green roofs, a watershed can approximate pre-development hydrology, which in turn benefits the system's ecological integrity (Prince George's County 1999; Roseen et al 2012). As a greater fraction of precipitation is rerouted through subsurface pathways, water reaches streams and lakes at a gentler pace. This slower discharge reduces destructive peak flows in

streams by up to 90% (Pagotto et al. 2000; Roseen et al. 2012). Reductions in flow volume also account for reductions in contaminant loads to streams. Furthermore, stormwater contaminants such as nutrients, suspended solids, organic compounds, and heavy metals are often treated in this process as there is greater potential for biodegradation and adsorption (Table 1; Pitt et al. 1999).

Pitt et al. (1999) reported that nutrients, pesticides, pathogens, heavy metals, and organic compounds common in stormwater all have low or low to moderate potential to contaminate groundwater following surface infiltration, suggesting that infiltration systems can reduce contaminant loads to streams. Two contaminants were found to have high groundwater contamination potential: enteroviruses and Cl^- salts. Wastewater is the primary source of viruses, the survival of which depends on the pH and ionic content of the solution (Pitt et al. 1999). As discussed in the previous section, Cl^- is a conservative contaminant, and is not easily purged from groundwater. Borst and Brown (2014) observed detectable levels of Cl^- below permeable pavement surfaces throughout all seasons, although no exceedances of the EPA drinking water guideline (250 mg L^{-1} Cl^-) were observed between April and December (i.e. non-salting months). These year-long Cl^- detections were attributed to salt sequestered in and below the pavement, and highlight the persistence of salt in the subsurface. Roseen et al. (2012) found that a de-icer application rate 25% of that used for conventional paved surfaces resulted in no difference in snow or ice cover on a permeable asphalt when compared with higher rates (50% and 100% of conventional)

Permeable asphalt (PA) is a permeable pavement technology[1] that owes its pervious nature to the omittance of fine particles from the pavement's aggregate mixture. This 5-10 cm layer is underlain by a stabilizing 'choker course' layer, consisting of 5-10 cm of crushed

[1]Other examples include permeable concrete and permeable interlocking concrete pavers

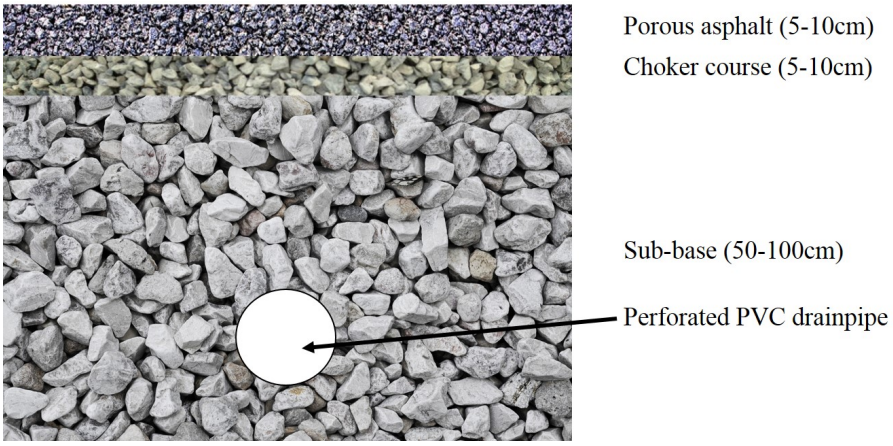

Figure 1.1: Cross section diagram of typical permeable pavement, showing upper infiltration layers and infiltrate reservoir. Native soil underlies this sub-base layer.

Table 1: Stormwater contaminant removal from stormwater infiltration practices (Pitt et al. 1999).

Stormwater contaminant	**Groundwater mobility**	**Abundance in urban stormwater**	**Groundwater contamination potential following surface infiltration**
Nutrients (NO_3^-, PO_4^{2-})	Mobile	Low/moderate	Low/moderate
Pesticides	Mobile	Low	Low
Organic compounds	Low/moderate	Common	Low/moderate
Pathogens	Varies based on species' oxygen tolerance, nutrient availability	Common	Low (high potential for enterovirus)
Heavy Metals (Ni, Cr, Pb, Zn)	Variable (sensitive to redox, pH)	Common	Low
Salt (Cl^-)	Mobile (conservative)	Seasonally high	High

gravel. A highly permeable layer of crushed stone underlies the asphalt and choker layers; this 50-100cm thick layer serves as a reservoir for infiltrate, as the native soil may have a slower infiltration capacity than the PA. Perforated PVC drain pipes are often installed to divert excess stormwater to nearby stormwater systems (Figure 1.1). Geotextile fabrics have been used to prevent migration of variably-sized soil and rock, however they can clog with sediment, reducing the overall efficacy of the PA (Boving et al. 2008; Roseen et al. 2012).

1.3 Winter de-icing

In winter months, the temperature of roads and sidewalks can fluctuate above and below the freezing point of pure water (0°C). De-icing agents are applied to the surfaces of roads and sidewalks to depress the freezing point of water. Any dissolved constituent will lower the freezing point of water, but Cl^- salts are used because of the cost and logistical convenience. In addition to the state department of transportation (CT DOT), municipalities, private organizations and individuals apply some variety of de-icing salt. On the state level, NaCl is the most commonly used de-icing agent, although smaller amounts (typically less than 2% by weight, annually) of $CaCl_2$ and $MgCl_2$ are also used when pavement temperature drops below 25°F (-3.9°C) (Mullaney et al. 2009; Cassanelli and Robbins, 2013; CT DOT 2013). Municipal and private salting practices vary in magnitude, method, and chemical of choice; therefore, it is challenging to assess trends at this level.

In the winter of 2006/2007, the CT DOT began pre-treating state roads with liquid salt brines, composed of 23% NaCl by weight (Mullaney et al. 2009; CT DOT, 2013). This prophylactic approach, called 'anti-icing' allows for a lower NaCl application rate of 35-50 kg NaCl per lane mile, compared to 90 kg solid NaCl per lane mile and prevents the formation of ice packs. This practice ostensibly reduces the need for subsequent applications. During and after snow events, solid NaCl is applied as a 'de-icing agent' to melt existing ice and prevent the worsening of icy conditions. This solid NaCl is often wetted with water or salt brine prior to application in order to minimize the bouncing or scattering of salt from pavement surfaces. Both

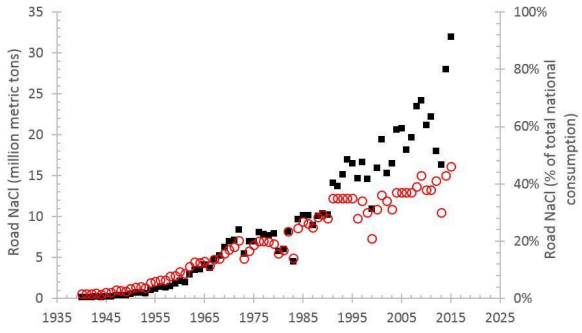

Figure 1.2: Annual road salt use in million metric tons is represented as black squares. Road salt use as a percentage of the total national salt consumption is represented as red circles. Data compiled from USGS mineral yearbooks, 1940- present.

anti- and de-icing methods are used during a typical storm, and Angel (2015) observed that a total of 3 de-icing treatments are typically applied to road surfaces on the UConn, Storrs campus. Based on these application rates, approximately 300 kg NaCl is deposited per lane mile during a single storm event. Assuming 13 storm events per year[2] , the annual salt load would equal approximately 4 tons per lane mile. However, estimates from highway officials range from 10-30 tons per lane mile annually (Mullaney et al. 2009), which suggests that de-icing may occur more frequently on state roads than on the UConn campus.

1.3.1 De-icing trends

The recorded history of salt used for de-icing begins in 1940, when it was first noted in the USGS mineral yearbook. This history is summarized in Figure 1.2. Since then, the annual mass of de-icing salt has gradually increased (USGS mineral yearbooks; Cassanelli and Robbins, 2013). This trend could be attributed to the construction of the US interstate system and other new roads in the past 75 years. Additionally, the fraction of the nation's salt use applied in highway de-icing practices has also increased since the beginning of the practice, suggesting a rise in relative salt application rates.

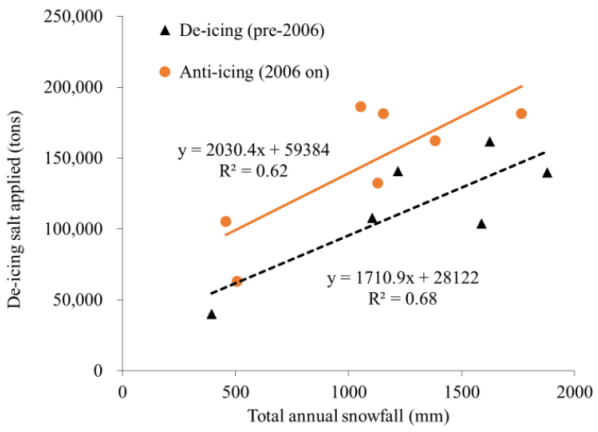

Figure 1.3: Annual de-icing salt application as a function of total snowfall, broken up by pre- and post-implementation of anti-icing. Data from Mahoney et al. (2015).

The Connecticut Academy of Science and Engineering recently published an analysis of winter de-icing practices for the CT department of transportation (Mahoney et al. 2015). The investigation found that the seven winters following the implementation of anti-icing[3] experienced 33.5% fewer weather-related car crashes than the seven

[2]Average of annual quantity of winter storms in CT from 2000-2016, (Mahoney et al. 2015)
[3]Anti-icing was first implemented during the 2006/2007 winter season

previous winters. The authors also acknowledge the relationship between a given season's total snowfall and vehicle crashes. The post-2006 period had 18% less average snowfall than the period before the beginning of anti-icing, indicating that the net reduction in crashes can be attributed to annual variability in winter precipitation, as well as the change in de-icing application procedures. The DOT highlights that total snowfall is a simplified representation of winter storms; they mention that other factors such as subfreezing temperatures, ice accumulation and refreezing events contribute to the severity of a winter and require additional Cl^- application (CT DOT, 2015). Regardless of the annual snowfall, additional de-icing salt is used after the shift to the anti-icing practice. In Figure 1.3, a year's total salt use is compared with that winter's severity (i.e. annual total snowfall). The application of de-icing salt is proportional to annual snowfall, and 50,000-100,000 additional tons of salt are used annually since the implementation of anti-icing (Mahoney et al. 2015). This increase is consistent with the trends documented in the USGS mineral yearbooks (Figure 1.2).

1.3.2 Environmental transport and fate of de-icing salt

Lakes and streams have background concentrations of Cl^- between 0 and 20 mg L^{-1}, (typically <5 mg L^{-1}) (Goldman and Horne 1983; Wetzel, 1975; Likens and Buso 2010). Sodium naturally occurs in freshwater at concentrations of <20 mg L^{-1} (Hem, 1985). Current findings indicate an upward trend in the salinity of freshwater in regions where de-icing activities occur such as the Northeastern and Midwestern US (Kaushal et al. 2005; Corsi et al. 2015). Both of these long-term studies reported that Cl^- concentrations largely fell below chronic aquatic toxicity levels during baseflow conditions. Shorter-term (i.e. less than 1-2 year study period) research has shown periodic spikes in river Cl^- concentration of 2,000-5,000 mg L^{-1} following runoff events and spring thaws (Meriano et al. 2009; Cooper et al. 2014). Streams located near major roads have significant risk of Cl^- levels in excess of the aquatic life criteria, especially during winter and spring seasons (Brown et al. 2015)

Decades of research document that de-icing salt can reach groundwater systems. Dennis (1973) showed that runoff from improperly covered salt stockpiles can infiltrate to the groundwater at concentrations of up to 2900 mg L^{-1} Cl^-. Angel (2015) showed that pulses of infiltrating melt-water can reach 6000 mg L^{-1} Cl^-. Current best management practices include storing salt reserves under cover, liquid brine applications, and calibrating salt spreaders to minimize input of Cl^- salts to the environment (CT DOT, 2013). However, elevated[4] groundwater Cl^- concentrations can be observed as far as 100m from roads due to normal de-icing applications (Bäckström et al. 2004). After acute pulses of Cl^- reach the water table, freshwater significantly dilutes the salinity (Dietz et al. 2016). Most groundwater in the glacial aquifers of the northern U.S. is still below the secondary maximum contaminant level (MCL) of 250 mg L^{-1} (Mullaney et al. 2009), although Cl^- concentrations in CT have steadily risen over the past century (Cassanelli and Robbins, 2013).

De-icing salt can also impact bedrock wells. An investigation of contaminated wells in Maine linked elevated Cl^- from de-icing to large increases in specific conductance during springtime thaws and recharge events, when the salts are most prevalent (Schalk and Stasulis 2012). In Connecticut, at least 10 private drinking water wells have been reported with high concentrations of ionic deicer components; Cl^- salt application was determined to be the cause in at least one case (Mahoney et al. 2015).

In a national investigation of Cl- in shallow groundwater, 2.5% of 1,329 wells had Cl^- above 250 mg L^{-1}, and the highest concentrations were typically found in urban aquifers (Mullaney et al. 2009). Geologic conditions across this large-scale study are highly variable, but Cl^- has been shown to accumulate in shallow groundwater-sheds in Toronto (Perera et al. 2013), Minneapolis/St. Paul (Novotny et al. 2009), and Pickering, Ontario (Meriano et al. 2009).

Once Cl^- percolates to an overburden aquifer, the ions will tend move conservatively with groundwater flow; some Cl^- will reach bedrock fractures, and some will be transported to stream systems as a component of baseflow. Meriano et al. (2009) found baseflow Cl^- of

[4]i.e. greater than 20 mg/L

greater than 500 mg L^{-1} in an urban stream in Ontario. This corresponds to similar findings by Perera et al. (2013), who measured Cl^- during baseflow periods in a Toronto stream. Perera et al. (2013) described the shallow urban aquifer as a dual-porosity formation, consisting of (a) native overburden media and (b) epikarst,[5] or highly permeable, disturbed units formed during excavations, the construction of utility trenches or other underground development. Baseflow contributions from the higher permeability portion of the aquifer reached the stream first with relatively high Cl^- concentration (<500 mg L^{-1}). During spring thaws and subsequent rain, freshwater flushes Cl^- from this disturbed component of the aquifer. By late summer, Cl^- ions were more homogeneously distributed in the aquifer and the groundwater Cl^- contribution to the stream stabilized at 250-300 mg L^{-1} (Perera et al. 2013). In this watershed, consistent Cl^- input from groundwater recharge exceeds the level of chronic aquatic life toxicity criterion.

In lakes, high-density saline water from runoff or groundwater settles at the bottom depths, forming a Cl^- gradient. This chemo- or halocline was of sufficient magnitude to inhibit vertical mixing in a bay near Rochester, NY (Bubeck et al. 1971). This prolonged stagnation resulted in a nutrient deficit, however this is the only reported instance of this phenomenon (Transportation Research Board 1991). A 40-year study of the salinity of a roadside lake (Mirror Lake, Woodstock NH) identified an increase in outlet Cl^- concentration from less than 1 to 4 mg L^{-1} (Likens and Buso 2010). While this change in the lake's 'solute array' may not present aquatic toxicity threats or prevent vertical mixing, increased Cl^- export from head-water-bodies could have cumulatively negative impacts downstream.

1.3.3 Ecological impacts

As melting snow and ice infiltrate to soils, salt enters the groundwater in the form of dissolved Na^+ and Cl^- ions. The most immediate effect of this is salt stress: additional aqueous ions reduce the osmotic water potential, hindering the ability for most plants and microor-

[5]Originally defined in Garcia-Fresca (2007)

ganisms to uptake water (Yan et al. 2015). Furthermore these ions can strip micronutrients such as Ca^{2+}, Mg^{2+} and $NH_4{}^+$ from soil particle surfaces by processes such as cation exchange and ligand complexation (Norrström 2005). In the same manner, toxic metals such as As, Pb, Zn and Hg can also be leached from soils (Norrström and Jacks; 1998, Sun et al. 2015). The ecological impacts of these changes will be discussed in this section.

The aquatic life criteria for Cl^- was established based on LC_{50} values for several species of fish, amphibians, and aquatic invertebrates (USEPA, 1986). Sensitivity to salt is highly variable among species. Siegel (2007) reported that fathead minnow is a salt-sensitive species, with a LC_{50} of 874 mg Cl^- L^{-1}. In comparison, the LC_{50} for brook trout is 30,330 mg Cl^- L^{-1}, or nearly double the Cl^- concentration of seawater. It is expected that the more salt-tolerant species will dominate in increasingly saline water bodies, presenting a threat to biodiversity. For example the survival of spotted salamander larve (*Ambystoma maculatum*) is inhibited at moderate specific conductance (500 μS cm^{-1} (Karraker et al. 2008). *A. maculatum* is a robust indicator of ecological health; due to its reproductive frequency, limited home range, and broad geographic distribution, changes in population size can be attributed to local environmental changes.

Curiously, the EPA's Quality Criteria for Water (1986) does not mention microorganisms in its rationale for salinity standards. These organisms are found in nearly all freshwater systems and are critical to the survival of higher-order organisms across the food web. The majority of microorganisms cannot tolerate salinity levels above 1-1.5% NaCl (1,000-1,500 mg L^{-1}) but some have biological methods of adapting to changes in salinity (Larsen, 1986). In order to maintain the necessary ionic balance across their cell membrane, these halotolerant organisms produce additional organic salts during periods of elevated salinity (Hagemann, 2011). These bacteria (and cyanobacteria) are encountered in estuarine regions where tides and storms create a variable salinity regime. It follows that under saline conditions, the composition of microbial communities would shift to favor the halotolerant species. Aquatic salinization could have detrimental implications for nutrient cycling

(Hopfensberger et al. 2014) and evolutionary impacts for organisms higher in the food web (Brady 2012).

Plants cannot respond to changes in salinity as effectively; extended exposure to salt can inhibit water uptake, growth and eventually result in mortality. Dead vegetation is commonly observed adjacent to roads or sidewalks to which de-icing salt is applied. The toxicity threshold varies among plant types; wetland vegetation is negatively impacted[6] at 300 mg Cl^- L^{-1}, woody vegetation is slightly more tolerant (836 mg L^{-1}), and herbaceous plants are most tolerant (2500 mg L^{-1}) of saline water (Siegel 2007).

1.4 Environmental radionuclides

1.4.1 A note on units

Since M. Becquerel's and Mme. Curie's discovery of radiation in the late 19^{th} century, several units have been developed to describe quantities, concentrations and doses of radiation. For the purposes of this review, the unit systems commonly used in literature will be discussed.

The SI unit for radioactivity is the Becquerel (Bq), after Henri Becquerel for his discovery of radiation. This unit represents the activity of a mass of radioactive elements; an activity of 1 Bq indicates 1 disintegration per second (dps). Radiation analysis is performed by counting these disintegration events.

A curie (Ci) represents a large amount (3.7×10^{10}) of disintegration events. While non-SI, this quantity is not arbitrary; it refers to the number of disintegrations that occur during one second in 1 gram of pure radium-226. However, naturally occurring radioactive material is rarely concentrated to this extent. Instead, data are typically presented in picocuries (pCi, $Ci\times10^{-12}$) (Hem, 1985).

The EPA regulations concerning radioactive elements use units of picocuries per liter (pCi L^{-1}). This unit is analogous to mass concentrations, but more accurately describes

[6]Lowest observed effect level, LOEL

the activity of a particular element per unit volume. One pCi L^{-1} of ^{226}Ra is equivalent to 27.3 pg of that element per liter of gas or liquid. A similar unit (pCi kg^{-1}) refers to the activity of a particular element per kilogram solid mass. In uncommon situations of abnormally high radiation (i.e. a recently-dropped nuclear weapon) the energy of ambient atmospheric radiation is expressed as coulombs per kilogram.

The abovementioned units are derived from the phenomenon of radioactive decay. In the context of human health, another system of units is used. The gray (Gy), a SI unit, is a measure of an absorbed dose of radiation energy per unit mass (J kg^{-1}). The Sievert (Sv) describes the degree to which an absorbed dose of ionizing radiation (Gy) can induce carcinogenic cell mutations or genetic damage. For a given tissue in a given organ, greys and Sieverts are proportional. However as different organs have different propensities for radiation-induced damage, the Sievert is used to express 'equivalent dose.'

1.4.2 Radon

Radon (Rn) is a radioactive, noble gas that rises from the earth's surface to the atmosphere in trace concentrations. This phenomena, commonly referred to as exhalation, is ubiquitous across the planet. The most stable naturally occurring isotope of Rn is ^{222}Rn, which has a half-life of 3.82 days. ^{218}Rn, ^{219}Rn and ^{220}Rn also occur in trace quantities; these isotopes have half-lives on the order of milliseconds to seconds, and will not be discussed further.

Due to its relatively short half-life, nearly all of the planet's Rn has been generated from decay of radium (Ra) isotopes in the uranium decay series. Therefore, Rn can only be formed near Ra bearing soil grains. Within the molecular structure of the solid grain, Rn atoms have a diffusion coefficient ranging from 10^{-31} to 10^{-69} m^2 s^{-1} (Nazaroff 1992). Alone, this inhibitive molecular diffusivity would render Rn particles immobile. However in the formation of Rn, radium releases an alpha particle and an initial energy of 86 keV (Singh et al. 2011). This is a typical energy value for a radioactive decay process, however most molecular bond energies are less than 1 keV. It follows that this burst of energy can

shatter the local crystal structure of soil grains, thereby enhancing the initial mobility of the daughter nuclide. This nascent burst of energy and the corresponding mobility are termed 'alpha recoil.' The recoil range of Rn atoms varies as a function of molecular opposition. For instance: in quartz, Rn can travel 0.034 μm; in water its range is 0.077 μm; in air Rn particles moves 53 μm due to alpha recoil (Sakoda et al. 2011). In some cases, these recoil events enable Rn particles to leave, or 'emanate' from soil grains. In other cases, the parent nuclide is embedded too deep in the grain or the daughter atom recoils into an adjacent grain; in these situations the newly formed Rn particle is sequestered amid the molecular structure of the grain.

The ratio of the amount of radon atoms emanated to the total Rn generated per unit soil mass is known as the emanation coefficient. This quantity theoretically ranges from 0 (all Rn sequestered) to 1 (all Rn emanated) but typically ranges from 0.05-0.70 (Nazaroff 1992) with an average of 0.20 in soil and 0.13 in rock (Sakoda et al. 2011). Perhaps counterintuitively, soil moisture increases the emanation coefficient of Rn. Nazaroff (1992) attributes this trend to the fact that average pore dimensions (0.5-50 μm) are typically less than the recoil range of Rn in air. Therefore, a Rn atom is more likely to terminate its recoil in a wet pore as the water can absorb the recoil energy more effectively than air.

The Rn particles that successfully emanate from their parent nuclides tend to seek a gaseous phase. With a dimensionless Henry's law coefficient[7] K_H of 0.35, Rn readily partitions from the liquid to gaseous phase. At this point the transport of Rn is governed by the atmospheric forces responsible for soil gas motion; some of the Rn will remain belowground for its lifespan, some particles will reach the surface. The phenomena of Rn permeating out from the ground surface is referred to in the literature as exhalation, or flux. Low levels of Rn exhalation occur across the globe; estimations of the average terrestrial Rn exhalation rate range from 0.35-0.57 pCi m^{-2} s^{-1} (Wilkening et al. 1972, Hirao et al. 2010). In the oceans, the average flux density is 0.001 pCi m^{-2} s^{-1}, however bands of slightly higher flux (maximum of 0.004 pCi m^{-2} s^{-1}) occur at latitudes of 0°, 20°N, and 60°S (Schery and

[7]Partition coefficient for Rn in freshwater at 25°C, liquid to gas ratio

Huang 2004).

The magnitude of Rn exhalation varies spatially, seasonally, and temporally. The spatial variation is due to availability of parent atoms in the subsurface; higher flux is observed in regions of abundant naturally-occurring radioactive material (NORM). For instance, the greatest Rn exhalation was observed in Australia (0.91 pCi m^{-2} s^{-1}), and the smallest flux was observed in northern North America (0.22 pCi m^{-2} s^{-1}) (Hirao et al. 2010). Other site-specific factors such as the overburden's permeability and thickness influence Rn flux. Greater flux is observed in areas of shallow bedrock and high permeability as the path between the surface and the source of Rn is shorter and less constricted. Soil moisture inhibits Rn flux as the diffusivity of a particle is lower in water than it is in air. Frozen soil will prevent exhalation entirely as gas flow is cut off between the soil vapor and the atmosphere (Nazaroff 1992). Diffusion will increase with temperature, and the solubility of Rn in water decreases with temperature. Therefore, Rn exhalation is greatest in warmer periods of the year. Globally, seasonal variations account for fluctuations of $\pm 10\%$ from the mean exhalation rate (Hirao et al. 2010) although these variations may be larger or smaller in regions with more or less seasonality. Variations in atmospheric pressure will induce advective flow as the soil gas equilibrates with these barometric changes. A greater pressure gradient induces more flow; alternating periods of high and low pressure facilitate the exhalation of Rn from the ground. Due to its 3.8 day half-life, the majority of exhaled Rn originates in the unsaturated soil or shallow water table. Most Rn that forms deeper below the water table surface remains there for its lifetime due to its low diffusivity in water.

Exhalation represents the primary source of human exposure to Rn. On most of the earth's surface, the exhaled Rn presents negligible health risk as it is diluted to negligible levels in the atmosphere. However this degree of dilution is not possible in buildings; Rn that diffuses through building foundations can accumulate at harmful levels. Additionally, wells and plumbing can serve as a conduit between deep-aquifer Rn and human lungs. Ingesting Rn-bearing water is not of itself a health concern, but due to the volatility of the element

Rn can diffuse out of faucet streams when turned on, especially in showers or other hot water streams.

The toxicity of inhaled Rn results from its decay; the daughter elements and the alpha radiation released in their formation can damage sensitive lung tissue (National Cancer Institute, 2011). Recent statistics estimate that long-term Rn exposure is the second leading cause of lung cancer (Robertson et al. 2013, Darby et al. 2001). The EPA and the U.S. surgeon general recommend remedial action in buildings with gaseous Rn levels above 4 pCi L^{-1} (150 Bq m^{-3}) due to the inhalation hazard.

1.4.3 Radium

Radium is formed in the decay of uranium and thorium isotopes, and is present in the earth's crust in trace concentrations. The naturally occurring isotopes of radium (Ra) are ^{226}Ra, ^{228}Ra, ^{223}Ra and ^{224}Ra; these have half-lives of 1,600 years, 5.75 years, 11.4 days and 3.6 days respectively. ^{226}Ra is the sixth product in the decay of ^{238}U, and is the most abundant isotope. ^{228}Ra and ^{224}Ra are the second and fifth products in the ^{232}Th decay series. ^{223}Ra is a daughter product in the ^{235}U decay series, and is the least common of all Ra isotopes.

Ra is most abundant in shale, slate, clay rock and granite formations; the concentration of Ra in overburden soil is largely dependent on that of the parent rock. Globally, the Ra content of soil can range from 100-3,400 pCi kg^{-1}; typical deciduous and mixed forest soils in the US exhibit a narrower range of 500-1,100 pCi kg^{-1} (IAEA 2014). Areas in and around radionuclide mining operations can exhibit higher[8] Ra activity than typically encountered. After formation, Ra tends to diffuse out from the rock matrix where it sorbs to the weathered (i.e. oxidized) surface of fractures. As the diffusion rate of Ra exceeds its decay rate, a gradient of Ra forms within the matrix, increasing toward the rock/water interface (Wood et al. 2004). The charge density of these fracture surfaces is such that

[8]Ra activities of 800,000 pCi kg^{-1} were measured in soil near a Uranium mine in Tapira, Brazil (IAEA 2014).

Ra cations are bound very tightly; this is reflected by a very high solid/liquid distribution coefficient (Tamamura et al. 2014).

The occurrence of Ra in groundwater is dependent on the presence of its parent isotope, its solubility in the water, and the age and chemical composition of the water. The variability of these parameters often explains why Ra is rarely in secular equilibrium[9] with parent radionuclides in the liquid phase. Ra can enter the liquid phase due to mineral dissolution (especially in sulfate rich aquifers) or desorption. As is typical for most adsorbent compounds, the liquid/solid partition coefficient (K_D , mL g^{-1}) for Ra varies greatly with site-specific parameters such as mineral type, pH and ionic strength. A lab-scale adsorption experiment (Tamaramua et al. 2014) demonstrated that the K_D of Ra on two clay minerals decreases by 4 orders of magnitude with increasing NaCl concentration. In the aqueous phase, the predominant species of Ra is the uncomplexed Ra^{2+} ion, however complexation will occur in solutions with ionic strength greater than 0.1 M (Langmuir and Riese, 1985). The primary complexes that form are RaSO 4 and $RaCl^{+}$; intuitively, the relative abundance of either complex depends on that of the respective ligand. However, $RaCl^{+}$ dominates over $RaSO_4$ at higher TDS values (Sturchio et al. 2009). These findings match field observations; an investigation of 1,270 drinking water samples across 45 states identified that Ra most commonly occurred in aquifers with high levels of dissolved, competing ions (Szabo et al. 2012). Wood and others (2004) demonstrated the capacity for saline solution to induce ion exchange at fracture surfaces, thereby releasing Ra into groundwater. In this study, a $MgCl_2$ brine was injected into a bedrock well, then extracted from the rock formation in a well 13.9m away. A release of both U and Ra to the water correlated with the plume of brine; this was attributed to the occurrence of ion exchange between Ra and Mg ions at weathered rock surfaces (Wood et al. 2004).

Ra is a bone-seeking carcinogen; exposure to this element has been shown to cause health problems such as anemia, cataracts and cancer (ATSDR 1990). The quantity of Ra necessary

[9]Secular equilibrium refers to a condition in which the quantity of a radionuclide remains constant due to equal production and decay rates.

to induce these negative health effects is not well known. The EPA's maximum contaminant level (MCL) for Ra is set at 5 pCi L^{-1} based on estimates of health risk (US EPA 2000).

1.5 Conclusion

As paved surfaces continue to be treated with salt in winter months, continued salinization of surface and groundwater systems will likely be observed. While the transportation and safety benefits of the practice are significant, this salinization has many negative ecological consequences: surface water systems are approaching chronic aquatic toxicity thresholds for Cl^-, the growth of roadside vegetation is stifled due to an increase in soil salinity, elevated hardness and conductivity are observed in roadside aquifers. This subterranean consequence presents increased treatment costs (i.e. water softeners) and human health concerns (larger Na^+ loads) for those who depend on groundwater as a drinking water source. Previous research has documented these trends of salinization in roadside groundwater; this study seeks to investigate the long-term transport and fate of groundwater salinity further downhill from the source. Additionally, the occurrence of Ra in naturally saline aquifers is well documented. The objectives of this research were to (a) investigate the long-term behavior of Cl^- in groundwater surrounding a permeable asphalt parking area and (b) assess the possibility of a connection between unsafe levels of Ra and anthropogenic salinity in groundwater. The fulfillment of these objectives will give policy makers and transportation officials further insight when accounting for costs and benefits of winter de-icing.

Impacts of de-icing salt contamination of groundwater in a shallow urban aquifer

2.1 Introduction

A gradual salinization of surface- and ground-water bodies has been observed due to anthropogenic de-icing practices (Kaushal et al. 2005, Cassanelli and Robbins 2013, Perera et al. 2013, Cooper et al. 2014). Winter de-icing refers to the practice of applying salt to paved surfaces in order to reduce the freezing point of water, thereby preventing the formation of ice. The chemical composition of de-icing salt may vary between applicators or under different temperature conditions, but sodium chloride (NaCl) is typically the principal component of salt applied by the Connecticut Department of Transportation (CT DOT) (Mahoney et al. 2015) and the University of Connecticut (UConn) (UConn Landscape Services, personal communication, 2016). The safety benefits of these practices cannot be overlooked; between 2001 and 2010, 500 fewer winter-season car crashes were observed during the later 5 years, in which de- and anti-icing and methods were employed (Mahoney et al. 2015). However when coupled with the concern for the salinization of roadside soil and groundwater, the need for a robust life-cycle-analysis of the costs and benefits of this practice becomes apparent.

In order to assess the long-term fate and behavior of salt in groundwater, naturally saline

aquifers were investigated in the literature review. Detections of Radium (Ra) were proportional to salinity in Midwestern and North Carolina aquifers (Sturchio et al. 2001, Vinson et al. 2009), as well as in a review of 15 principal aquifer systems across the US (Szabo et al. 2012). Additionally, the volatility of dissolved gases such as radon (Rn) is enhanced in electrolytic solutions, due to a phenomenon known as salting-out. This increased volatility (or decreased solubility) of Rn was modeled by Schubert et al. (2012). The possibility that anthropogenic salinity could increase human exposure to these radioactive, carcinogenic elements has not been investigated. In this thesis, data will be presented that verify this possibility.

Additionally, the nature of de-icing salt contamination at this site will be re-investigated to append the analysis presented by Angel (2015). Since this initial site characterization, three wells have been installed and 15 months have passed. This increased spatial and temporal resolution allows for further exploration of the potential for de-icing salt contamination in shallow urban aquifers.

2.2 Methods

2.2.1 Study site

The site investigated in this study encompasses an area of approximately 7,250 m^2 ($\sim$1.8 acres) on the University of Connecticut Storrs (UConn) campus in Storrs, CT USA (Figure 1). The site consists of an 860 m^2 permeable asphalt parking lot and approximately 325 m of impermeable roads and sidewalks. The overburden soil surrounding the permeable asphalt consists of highly compacted glacial till and native sandy silt. The site is underlain by the Hebron Gneiss formation at a depths ranging from 2.1 to 5.2m.

Six overburden monitoring wells were installed at the site to understand changes to its hydrogeology. Wells DG-1, DG-2 and UG-1 (Figure 2.2) were installed in 2014 to assess

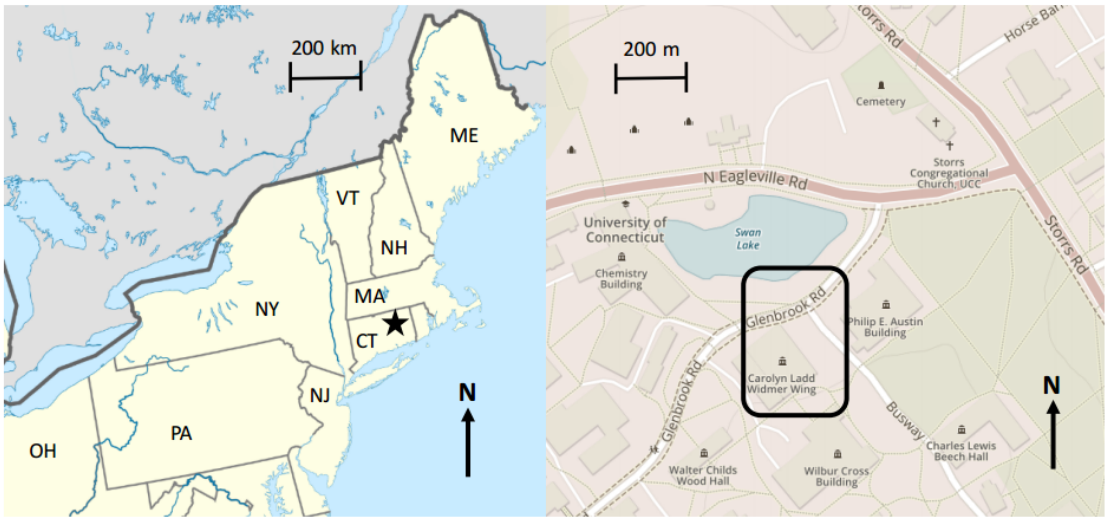

Figure 2.1: Location of the study area within the Northeastern US (denoted by black star on left), and location of study site within UConn campus (circled on right).

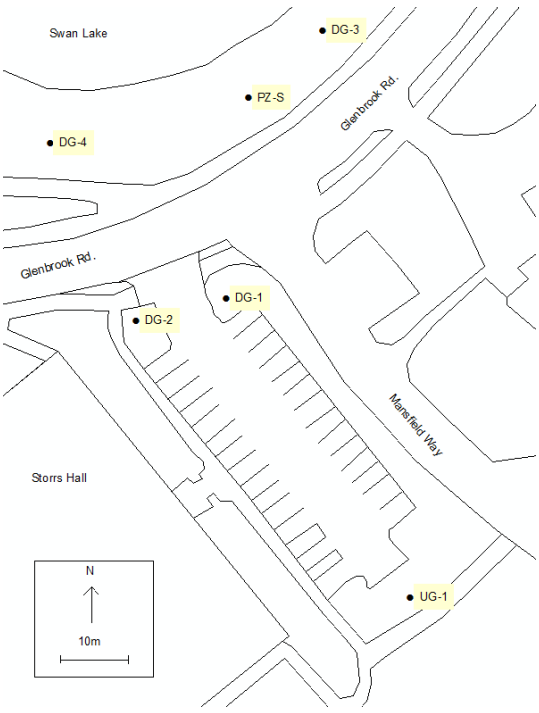

Figure 2.2: Diagram of the study site, well locations are labeled and denoted by black circles. PZ represents a nest of 3 piezometers.

differences in groundwater quality upgradient (UG) and downgradient (DG) from the porous asphalt (Angel 2015). Located North of Glenbrook Rd., the three wells labeled DG-3, DG-4 and PZ were installed in October 2015 to assess the fate of Cl^- as it travels further down along the hydraulic gradient. The sediment cores were preserved in jars and their respective coring logs are included in the appendix. PZ is a set of 3 nested piezometers, each drilled to a discrete depth. The purpose of this cluster was to assess the vertical flow direction, as well as vertical variations in chemical constituents. After installation, each well was purged by low flow sampling to remove fines from the pre-packed well screens. The installation of an additional upgradient well was attempted approximately 50 m south of UG-

1, however the location was abandoned after drilling through 7.3 m of dry glacial till. A portion of the core sample from this location was retrieved (2.4-6.1 m below grade) and archived.

Table 2.1: Monitoring well specifications (distances are approximate).

Well ID	**Surface elevation (m AMSL)**	**Depth (m)**	**Intake length (m)**	**Location/description**
UG-1	189.91	5.18	1.52	3m Southeast of the PA
DG-1	188.12	5.18	1.52	1m North of the PA
DG-2	188.18	5.18	1.52	3m Northwest of the PA
DG-3	184.51	2.44	1.52	North of Glenbrook Rd. Easternmost location
DG-4	186.96	3.96	0.91	North of Glenbrook Rd. Westernmost location
PZ-S		2.13	0.91	North of Glenbrook Rd. cluster of 3
PZ-M	184.95	3.05	0.30	piezometers installed to discrete depths
PZ-D		3.96	0.30	
WB-1	188.88	6.71	3.05	100m South of PA, not pictured in Figure 2.2

PA: Permeable asphalt

2.2.2 Groundwater quality monitoring

Long-term monitoring for salt contamination of the site began after well installation and development. Each well was equipped with an Instrumentation Northwest, Inc. (INW) AquiStar® CT2X pressure transducer/specific conductance sensor and data logger. Before installation, the conductance probes were calibrated to a reference solution of 2000 μS/cm. Pressure transducers were calibrated in the well to manual water level measurements taken with a Solinst® water level sounder. The sensors were programmed to record relative water level, conductance, and temperature on a 10-minute interval. Data records were downloaded from each sensor on a monthly to bi-weekly basis. In the piezometer nest, a sensor was installed in the shallowest well (PZ-S) in order to monitor the water quality of the top 4 feet of the water table.

Water samples were collected by low flow sampling on four dates between November 16 and December 18, 2015 in order to quantify the relationship between Cl^- and specific conductivity. These samples were added to the existing relationship developed by Angel (2015)

for this site. Stagnant water was removed from the well casing using a peristaltic pump at rates under 120 mL/min. Samples were analyzed for Cl^- with an ion specific electrode (ISE) using EPA method 9212 (USEPA, 1991). Additionally, the specific conductance of each sample was measured using the INW sensor in the well from which it was obtained.

2.2.3 Sampling and analysis

Between 1-3 March, 2016, a groundwater sample was collected from each well by low flow sampling for analyses of major dissolved cations (Na^+ ,Ca^{2+} ,Mg^{2+}), Cl^-, and radionuclides (^{222}Rn, ^{226}Ra, and ^{228}Ra). Samples for each analysis were also taken from Swan Lake and well WB-1.[1] As some of the target analytes are redox-sensitive or volatile, care was taken to monitor water quality parameters such as dissolved O_2 , redox potential and specific conductance while purging. After these parameters stabilized, 3.79 L of water was collected for Ra analysis, 500 mL was collected for cation analysis, 250 mL was collected for Cl^- analysis, and a 40 mL volatile organic analysis (VOA) vial was filled for Rn analysis. Metals were analyzed at the University Center for Environmental Science and Engineering (CESE) laboratory by ICP-OES using EPA method 200.7 (EPA, 2001). Rn and Ra were analyzed at the Connecticut Department of Public Health Laboratory using EPA methods 913.0 and 903.0/904.0, respectively.

An additional round of sampling was planned in early September, 2016 in order to assess the impact of seasonal variability. However at this time the site water table elevation was too low to collect representative samples, due to the annual variation and recent periods of drought. Despite pumping at low rates (<10 mL min^{-1}), water samples could not be extracted without excessive aeration. As Rn is a highly volatile element, this aeration would introduce substantial error in any Rn analysis. Unfortunately, the salting period began before the site could rise to a usable water table elevation, at which point assessing

[1]Not pictured in Figure 2.2, well WB-1 was sampled to obtain a background groundwater quality measurement, more distant from heavy salting areas on the campus. Details pertaining to this well are included in Table 2.1.

the degree of seasonal variability was futile.

2.2.4 Equilibrium vapor-phase Rn calculations

The equilibrium vapor-phase Rn concentrations were estimated using the method described in Schubert et al. (2012). This process uses the Weiss equation (eq. 2.1)...

$$\ln\beta = a_1 + a_2\left(\frac{100}{T}\right) + a_3\ln\left(\frac{T}{100}\right) + S\left\{b_1 + b_2\left(\frac{T}{100}\right) + b_3\left(\frac{T}{100}\right)^2\right\} \quad (2.1)$$

...where S is the salinity of the aqueous solution (TDS, g L^{-1}), T is the temperature of the solution (K), a_1, a_2, a_3, b_1, b_2 and b_3 are experimentally determined, element-specific coefficients derived for Rn in Schubert et al. (2012) and listed in Table 2.2 for reference. The β term is related to the Henry's law coefficient K_H as ...

$$K_H = \beta\frac{T}{273.15} \quad (2.2)$$

These two equations can be used to calculate the K_H of a gas based on the temperature and salinity of the liquid solution.

Table 2.2: Empirical parameters for Rn application of the Weiss eqn. derived in Schubert et al. (2012).

a_1	-76.14	b_1	-0.2631
a_2	120.36	b_2	-0.1673
a_3	31.26	b_3	-0.0270

2.2.5 Soil analysis

In order to assess the nature of salt transport through the soil column, samples from 30cm sections of two soil cores were analyzed for leachable Cl^- according to the procedure described by Sonmez et al. (2008) The Cl^- content of these samples was determined using an

ion-specific electrode according to EPA method 9212 (USEPA, 1991).

2.3 Results and discussion

2.3.1 Summary of climatological observations

The study period encompassed two full water years, and five months of a third (Oct. 2015-Feb. 2017). This period was substantially dryer than the 30-year normal (Table 2.3). During approximately one third of the study period, the departure was substantially below

Table 2.3 Monthly observed (Obs.) precipitation totals (mm) compared to normal monthly average (1981-2010) precipitation for Storrs, CT. Precipitation data from the NOAA station located in Storrs, CT *Station ID: USC00068138*

Month	**30-yr**	**2015***		**2016***		**2017***	
	mean precip.	Obs.	% Diff.	Obs.	% Diff.	Obs.	% Diff.
October	116.8	149.9	28.3	98.0	-16.1	120.1	2.8
November	116.1	107.4	-7.4	47.2	59.3	62.0	-46.6
December	106.9	100.1	-6.4	114.6	7.1	104.6	-2.1
January	96.3	85.3	-11.3	64.0	-33.5	82.6	-14.1
February	84.8	59.9	-29.3	140.5	65.6	43.7	-48.5
March	112.8	78.0	-30.9	68.3	-39.4		
April	115.1	101.9	-11.5	91.7	-20.3		
May	100.8	16.8	-83.4	77.0	-23.7		
June	113.3	197.9	74.7	55.9	-50.7		
July	100.1	46.5	-53.6	97.5	-2.5		
August	96.8	65.5	-32.3	108.5	12.1		
September	103.9	95.8	-7.8	39.6	-61.9		
Annual total	1263.7	1104.9	-12.6	1002.8	-20.6	413.0†	-20.7†

* Water year, beginning Oct 1 the previous year
† Total YTD

normal.[2] The relative lack of precipitation likely contributed to a lower overall water table elevation at the study site.

The snowfall of water year 2015 was nearly double that of the following winter, with approximately three times as many storms in 2015 than in winter 2016 (Table 2.4). Despite this inconsistency in annual winter severity, the hydrologic trend of salinization is more stable, which will be discussed further in subsequent sections. Angel (2015) calculated a

[2] i.e. less than the month's 25^{th} percentile

salt application rate of 0.077 kg m^{-2} per NaCl application, and an average of 3 applications per storm. By these estimates, approximately 5,200 and 1,800 kg NaCl were applied to the PA during winters 2015 and 2016, respectively. The rate of salt application to sidewalks is not known, as different equipment is used to treat these narrower paved areas. As discussed previously, the principal component of de-icing salt is solid NaCl. Rock salt is often treated with a liquid wetting agent prior to application in order to reduce scattering and clumping. The composition of this wetting agent may vary between private salt applicators; at this study site, the wetting agent consists of 60% calcium chloride ($CaCl_2$) and 40% lignin, a fibrous organic polymer derived from the cell walls of woody plants (Lebo et al. 2001). The

Table 2.4: Summary of monthly snowfall totals (mm precipitation as snow). Data from the NOAA station located in Storrs, CT *Station ID: USC00068138*

Month	**2015***		**2016***		**2017***	
	Obs.	N. Storms	Obs.	N. Storms	Obs.	N. Storms
November	127	2	0	0	0	0
December	43	1	33	1	203	3
January	658	7	183	2	264	3
February	777	1	368	4		3
March	257	4	122	1		
April	25	1	51	1		
Season total	1887	26	757	9	467†	8†

* Water year, beginning Oct 1 the previous year
† YTD

wetted form of this product is approximately 50% water, by weight, and 20-25 L is applied to treat 1 ton of rock salt. This converts to approximately 6-8 kg $CaCl_2$ per ton (907kg) solid NaCl, or less than 1% $CaCl_2$ by weight.

2.3.2 Soil analysis

After the installation of additional wells in fall 2015, selected samples from the soil cores were analyzed for leachable Cl^- in order to better understand salt transport through the unsaturated zone. The results of this analysis (Figure 2.3) were found to correlate with the soil density (i.e. permeability). The sections of higher density occurred between 1-1.5 and 3-4 meters below grade; peaks of Cl^- (195 mg kg^{-1}, 80 mg kg^{-1}, respectively) were

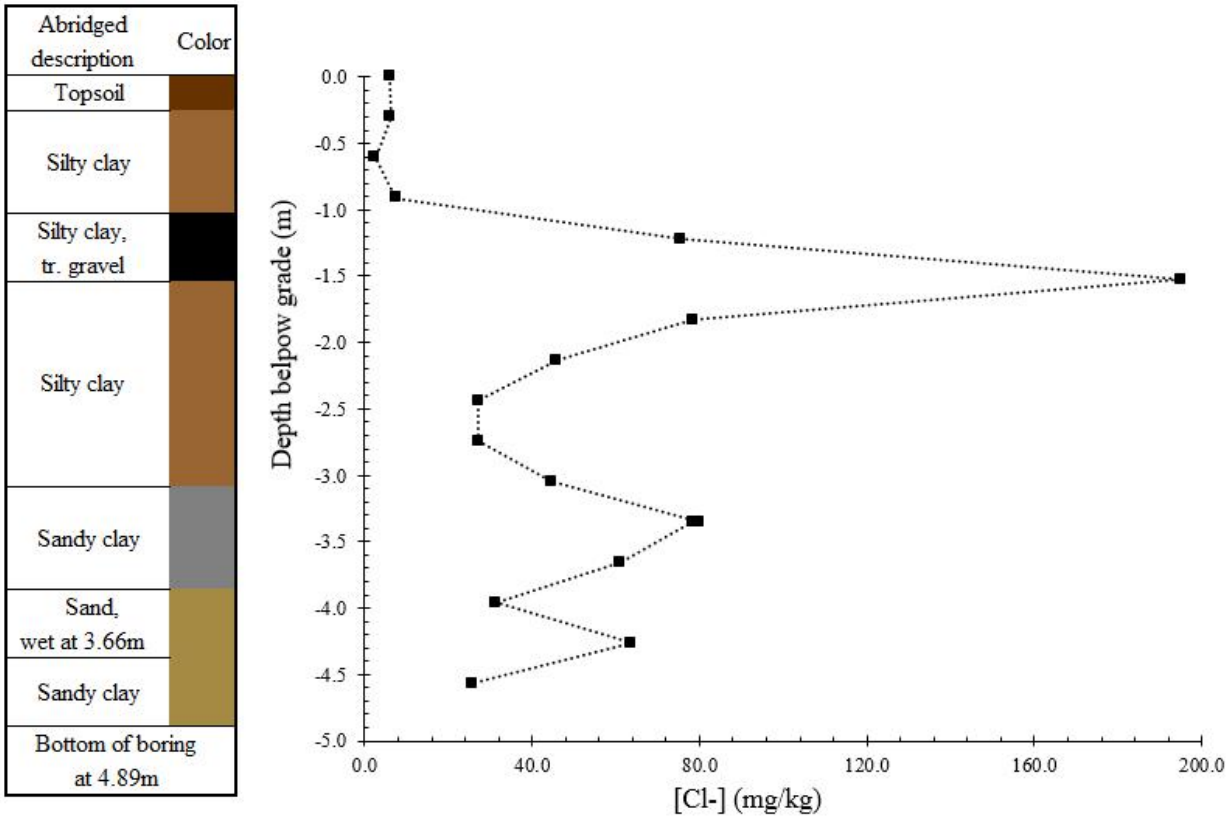

Figure 2.3: (Left) abridged description of soil core with soil color. (Right) down-core plot of soil Cl- content (mg/kg) from core sample taken at DG-4.

observed in these areas. This suggests that as Cl^- is transported downward to the water table by infiltrating precipitation, it accumulates in and above layers of lower permeability. That is, the rate of Cl^- input to these less permeable layers exceeds the rate at which it permeates downward. It cannot be concluded that layers are impermeable, as evidence of salt contamination is found deeper in the soil core. A third soil density gradient was observed 0.5m below the water table (4.2m below grade), with an accompanying peak Cl^- of 64 mg kg^{-1} .The general decreasing trend in soil salinity with depth (M L^{-4}), coupled with an estimate of the vertical infiltration velocity (L T^{-1}), could be used to approximate a site-specific salinization rate.

It's also possible that the lower soil salinity below the piezometric surface is due to the perpetual saturation at this depth. Due to the high solubility of the Cl^- ion, a smaller fraction of the salt is present in the solid phase.

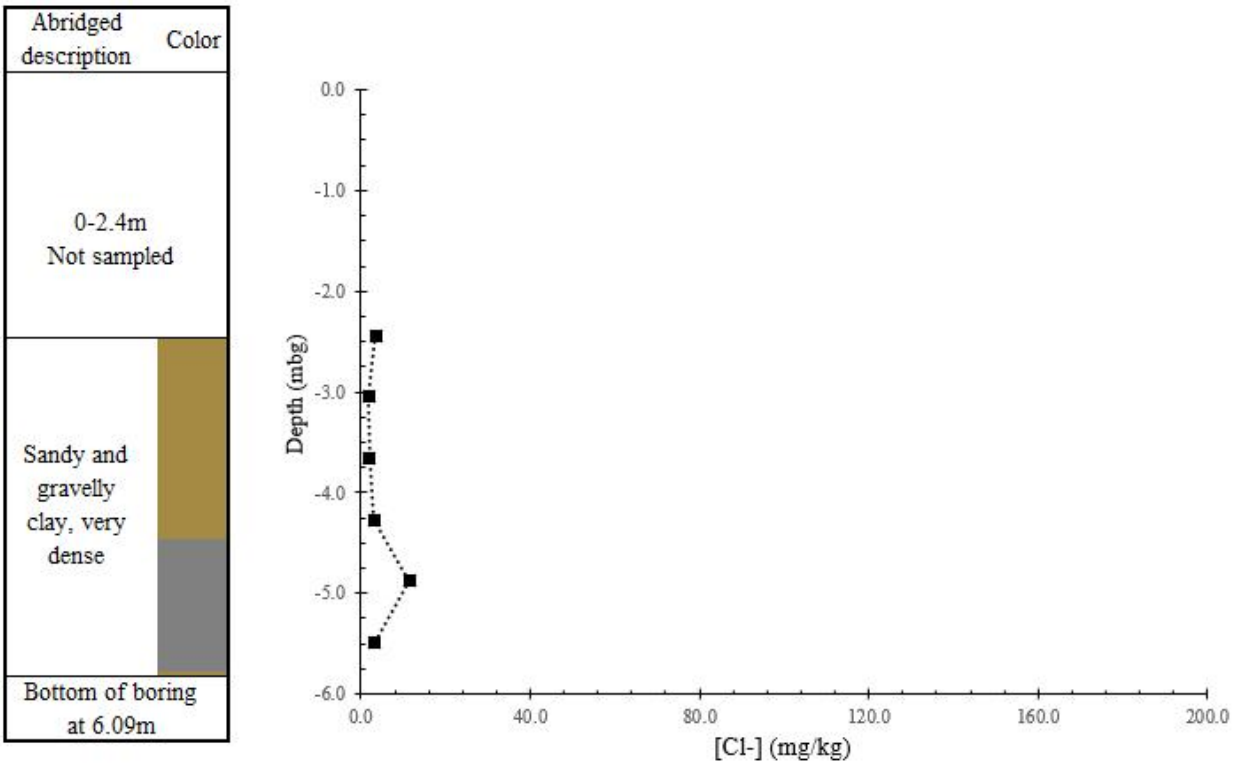

Figure 2.4: (Left) abridged description of soil core with color. (Right) down-core plot of soil Cl- content (mg/kg) from core sample taken at the prospective location of well UG-2, 50m south of (upgradient from) well UG-1.

Core samples from the attempted well UG-2 were also analyzed for Cl^- in order to quantify a possible background level of Cl^- at this site (Figure 2.4). Soil concentrations of Cl^- at this location are typically below 2 mg kg^{-1}, and all samples had less than 12 mg kg^{-1}. These measurements correspond with Cl^- observations from a Swedish forest soil (below 25 mg kg^{-1}) (Bastviken et al. 2007). The Cl^- content of soils is typically reported in units of kg ha^{-1}, and reaches a peak in the upper 40 cm of the soil profile due to its role in biological processes (Öberg 1998). In addition to these organic Cl^- sources, atmospheric deposition from the sea is seen as the primary input of salt to the soil. This phenomenon is manifested in historical (1894, 1902) Cl^- maps of Connecticut (Cassanelli and Robbins 2013), in which a gradient of groundwater Cl^- concentration decreases from 3 to 1 mg L^{-1} moving inland, with isochlors[3] parallel to the coastline. In soils, the abundance of Cl^- (relative to that

[3]i.e. lines of equal ceCl-

of organic carbon) is typically an order of magnitude less than that in surface water, and comparable to the abundance of phosphorus (Asplund and Grimvall 1991).

The relative lack of Cl^- at this location within the site is not surprising as there are no sidewalks or other sources of salinity this far upgradient; the location is near the top of a small hill. Additional sampling would increase the certainty of this conclusion, but under the assumption that the UG-2 core is representative of background soil salinity (i.e. not impacted by de-icing salt) it can be determined that soils with significantly higher Cl^- than this site are impacted by de-icing.

2.3.3 Site water table elevation

Water beneath this site tends to flow in a northwesterly direction (Figure 2.6), from the higher elevations at the southern end of the site, to the lower elevations at the north. At this point, groundwater can discharge to Swan Lake. The minimum water table elevation (WTE) did not fall below the elevation of the outflow weir of this stormwater detention pond (183.2 m).

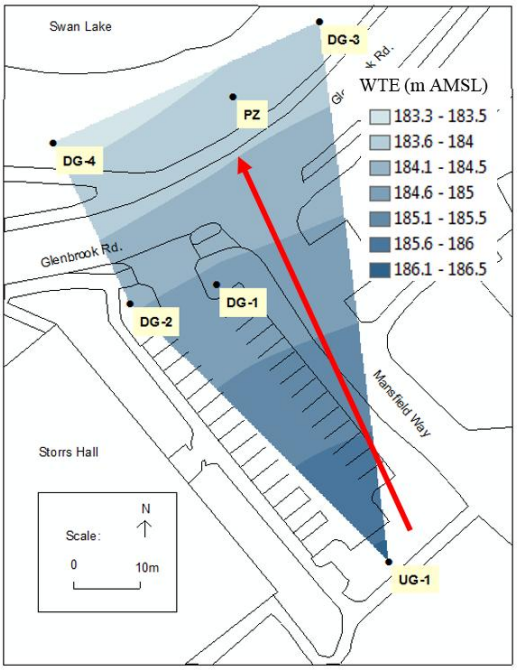

Figure 2.5: Study site on the University of Connecticut campus in Storrs, CT. The red arrow shows direction of groundwater flow during dry periods. Contours show the elevation of the water table. Black labeled and numbered dots are shallow wells. PZ is a piezometer cluster.

The water level in well DG-4 (top left of Figure 2.6) did not rise above the conductivity sensor within the well during the study. Thus, the water level readings in this well could not be accurately adjusted to a reference level. The long-term water level records at this location are used for assessing changes in relative water level, but not to make inferences about its relationship with neighboring wells. Therefore, the contoured water table surface shown in Figure 2.6 was generated using manual water level measurements taken on 3/3/16. The measurement in DG-4 was taken two hours after the sensor had been removed.

Presentation and discussion of the long-term water level observations will begin at the furthest up-gradient well (UG-1) then proceed downgradient.

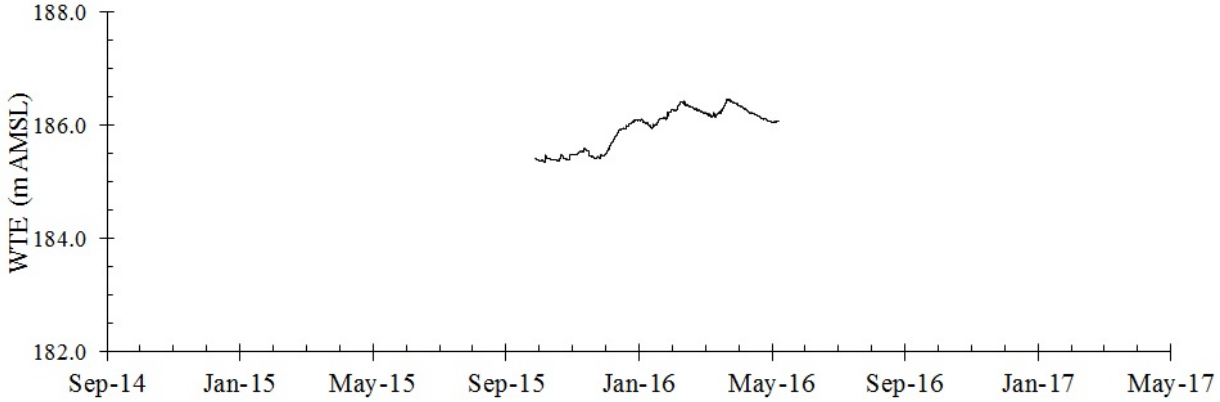

Figure 2.6: Water table elevation (WTE) over time in well UG-1.

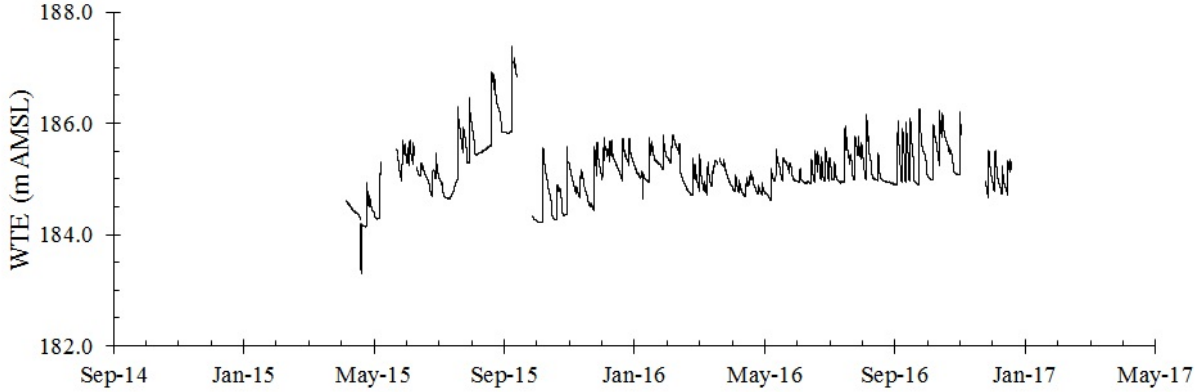

Figure 2.7: Water table elevation (WTE) over approximately 1.5 years in well DG-1. Gaps in the record are present when the sensor was removed for cleaning, had a dead battery, or during low-flow sampling.

UG-1

Although monitoring in this location occurred between 10/22/14 and 2/8/2017, accurate water level data for well UG-1 exist from 10/9/15 to 5/25/16. The sensor may have continued to record accurate water level measurements after 5/25, but this is the last date at which the sensor reading corresponded with a manual water level measurement. By the next measurement (6/20) a discrepancy was observed, which continued to grow for the remainder of the study. Therefore, the data after 6/20 were not included in this analysis.

The hydraulic conductivity at this location was measured at this location by Angel (2015); a K of 3.08×10^{-04} cm s^{-1} corresponds with the silty sand described in the location's boring log.

DG-1

Although monitoring in this location occurred between 10/22/14 and 2/8/2017, water table elevation records begin 5/1/2015. The peaks on this record correspond with storms and subsequent infiltration events. In winter months, a lag period was often observed between a storm and the peak water level; this lag was attributed to the time between a storm and the following warm period during which melting (and infiltration) occurred. During the period for which data exist for both DG-1 and UG-1, the water elevation is always lower at DG-1. This helps confirm the assumption that UG-1 is in fact up-gradient from all other wells.

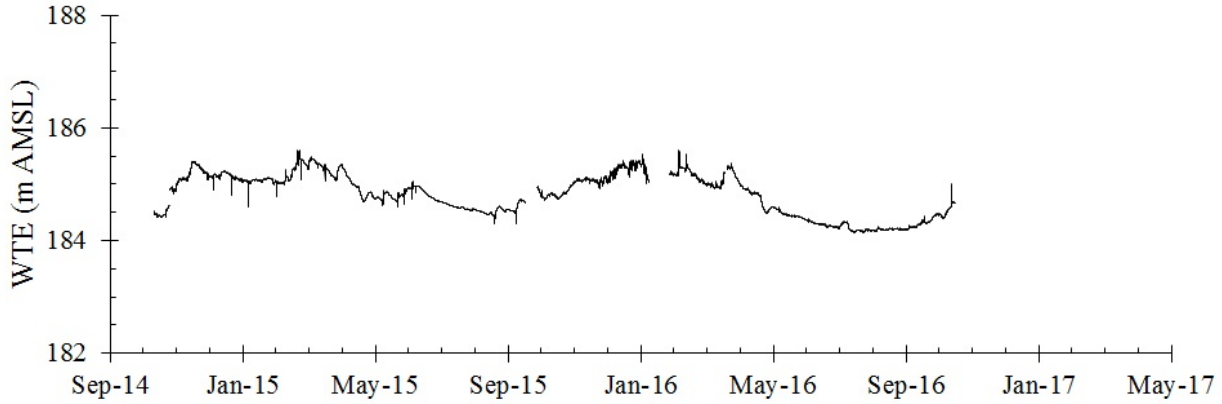

Figure 2.8: Water table elevation (WTE) over approximately 2 years in well DG-2. Gaps in the record are present when the sensor was removed for cleaning, or during low-flow sampling.

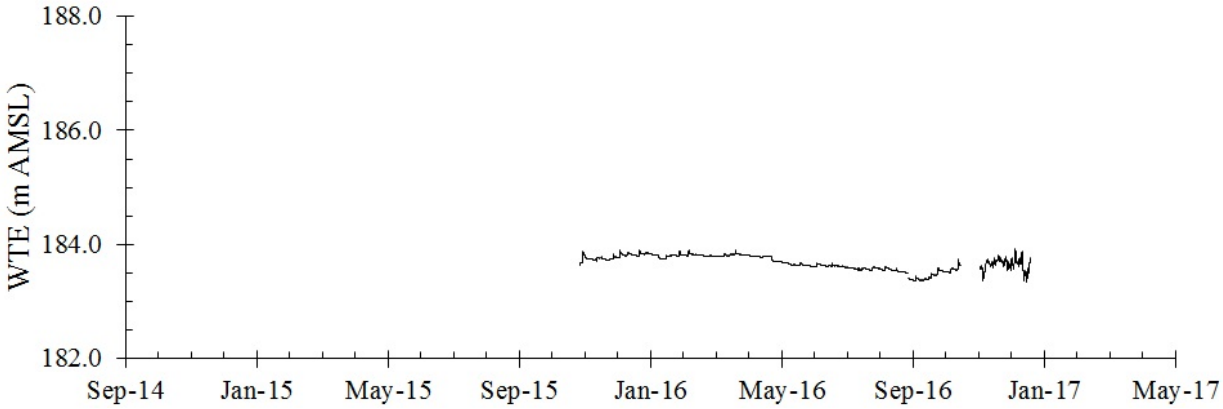

Figure 2.9: Variation in water table elevation (WTE) over approximately 1 year in the shallow well of the nested piezometer (PZ-S). Gaps in the record are present when the sensor was removed for cleaning, or during low-flow sampling.

DG-2

A record of the water level exists for this well from September 2014 to October 2016, or approximately 2 years. Water table elevation reaches a minimum during late summer (184.5 m AMSL), then starts to recover as evapotranspiration decreases in the fall, with a maximum elevation of approximately 185.5m. Storm events are less prominent here compared to well DG- 1, indicating a less direct hydraulic connection with the permeable asphalt, and a lower hydraulic conductivity.

PZ-S

Monitoring began at this location late fall 2015. The probe failed fall 2016. At this location, the sensor was installed in the shallowest of three piezometers. Throughout the year of monitoring, the water level varied by no more than 0.59m, reaching a minimum (183.3m AMSL) during the start of the 2017 water year. This is consistent with water level trends observed in neighboring wells.

Between the three nested wells, the hydraulic head gradient was typically less than 0.1m. During dry periods (i.e. no 48-hr precipitation) the water levels in both the shallow and deep wells were slightly higher (0.02m) than that of the middle-depth well. This indicates a small, upward gradient from the deeper groundwater and a small downward gradient of flow in the shallower, upper aquifer. During infiltration (i.e. in the period of time following a storm event) the WTE decreases from the shallow to the mid-depth to the deep piezometer, indicating a downward vertical component of flow throughout the entirety of the known aquifer.

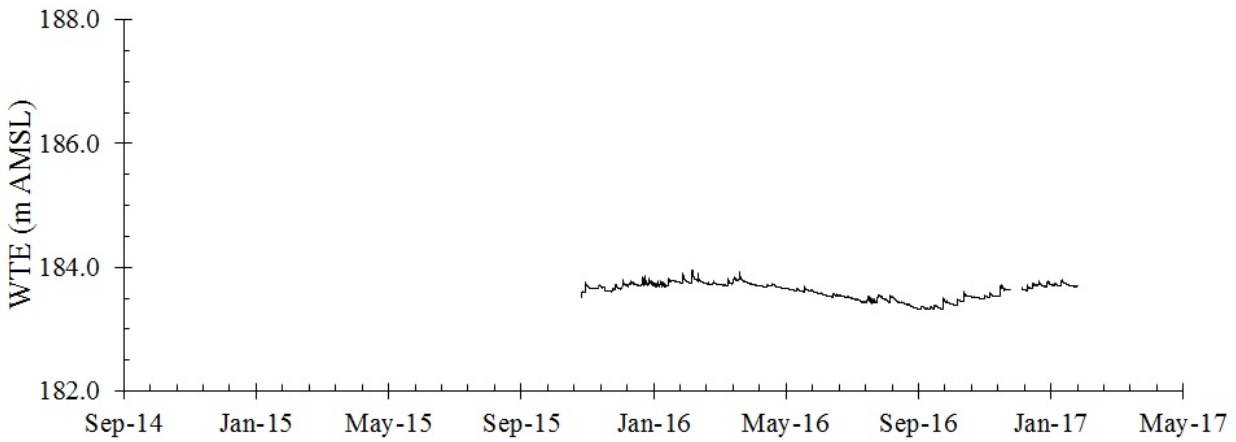

Figure 2.10: Variation in water table elevation (WTE) over approximately 1 year at well DG-3. Gaps in the record are present when the sensor was removed for cleaning, or during low-flow sampling.

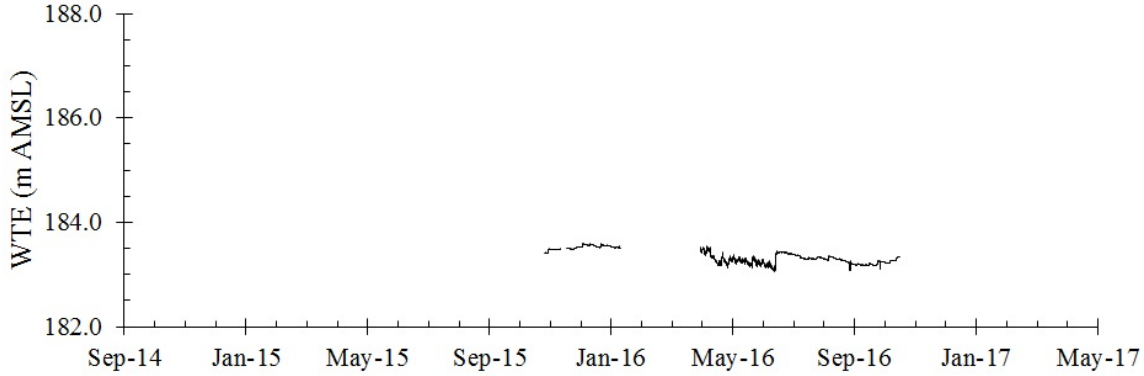

Figure 2.11: Water table elevation (WTE) over approximately 1 year at well DG-4. Gaps in the record are present when the sensor was removed for cleaning, or during low-flow sampling.

DG-3

Monitoring began at this well in fall 2015 and continued until February 2017. At this location, small spikes (<0.05m) correspond to precipitation events. These events are likely more apparent here than in neighboring wells (e.g. PZ-S, DG-4) due to the $\sim$ 1m difference between the ground and water level surfaces. The depth to water in this well is the shallowest of all wells on the site.

On an annual scale, the water level decreased from early March through the summer, reaching a minimum (183.3m AMSL) at approximately the beginning of water year 2017; at this point it resumed an increasing trend. The annual WTE range in this well is 0.64m.

DG-4

During the period of study, the water table at DG-4 did not rise to an elevation that could be measured with a water level sounder; the well's sensor was sufficiently submerged to collect readings, but they could not be verified nor corrected with manual measurements.

For the 10 months during which a functioning probe was installed, the water level varied by 0.54m. From April to late June 2016 an In-Situ probe was installed in the well, as the original probe had been sent back to the factory for repair. That original probe gave erratic water level readings starting early February 2016.

2.3.4 Groundwater quality monitoring

A note on units

As mentioned above, the water quality sensors used in this study measure specific conductivity, an assessment of the total electrolytic activity of the solution. Figure 2.5a shows the relationship between conductivity and Cl^- concentration. This correlation was developed using water sample data from Dietz et al. (2016) as well as samples collected during this study (n=71). The linear regression approximation is used to convert continuous (10-min) specific conductivity readings to Cl^- in the figures seen in subsequent sections.

Figure 2.5b was plotted in order to assess the relationship between specific conductiv-

ity and the known dissolved solids. While it is likely that additional ion species (i.e. HCO_3^-, SO_4^{2-}, K^+) were present in the samples, this relationship demonstrates that a conversion factor of at least 0.64 exists between the conductivity and total dissolved solids (TDS) for water at this site. As this factor varies between 0.55 and 0.75 in natural waters (Hem 1985), any additional ionic species were likely a marginal component of the TDS. For this relationship to have a slope of 0.75, the total ionic mass concentrations would only be 15% greater than the measured ionic concentrations.

2.3.4.1 Long-term monitoring: Chloride

The following figures document the changes in Cl^- concentration at each well in the study area. These figures were generated by converting the specific conductivity record to Cl^- according to the relationship depicted in Figure 2.5. As in the previous section, the discussion of each well will follow the path of the groundwater: starting at UG-1 and proceeding downgradient. Cl^- was used to describe the transport of salinity in general as it is a conservative component of groundwater; it does not undergo decay or chemical reactions but instead moves with the advective-dispersive groundwater flow.

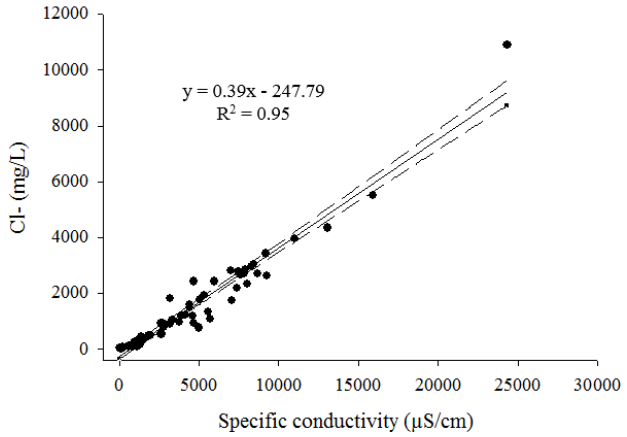

(a) Correlation between specific conductivity readings and Cl^- measurements (n=71). Dashed lines represent 95% confidence interval.

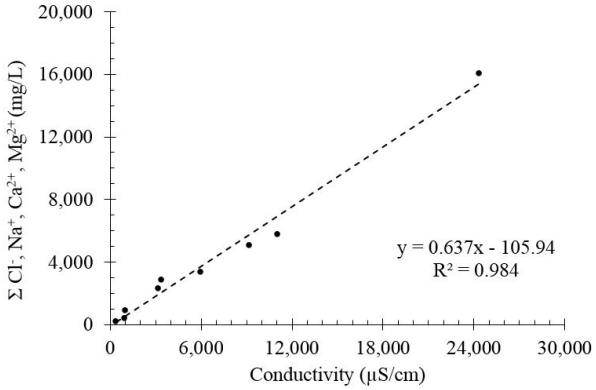

(b) Correlation between specific conductivity and total known dissolved ion species in groundwater samples.

Figure 2.12

UG-1

A record of the Cl^- concentration exists for this location between September 2014 and February 2017. Data do not exist for summer 2015 due to dead batteries in the sensor. Initial Cl^- measurements in this upgradient location reveal a background level of approximately 1000 mg L^{-1}. As previous investigations near the study area document typical Cl^- concentration below 100 mg L^{-1} (Cassanelli 2011), this initial finding suggests that de-icing salt from upgradient sources such as sidewalks has accumulated at this location. It is also possible that a temporary reversal of groundwater flow due to mounding below the porous asphalt has spread salt to this location, however this is unlikely given that no water level record at UG-1 falls below the WTE of any other well. Additionally, in a Cl^- tracer test conducted by Angel (2015) saline solution was applied to the PA; responses of Cl^- were observed in DG-1 but not in UG-1. This further verifies the northerly flow direction and lack of connection from the PA southward to UG-1.

The increase in Cl^- at the end of fall 2014 corresponds to the beginning of salting in the study area. During the salting period (i.e. November-April) the Cl^- concentration was around 3,000 mg L^{-1}; the sharp increase at the end of that season is attributed to a release of salt following the thaw of frost in the overburden. When monitoring resumed in October 2015, Cl^- had fallen to 1,200 mg L^{-1}, indicating that dispersion and dilution had occurred during the summer.

The well reached two Cl^- maxima during water year 2016, which occurred during February and June. The first peak corresponds with de-icing activities. The persistence of high Cl^- (3,200-4,000 mg L^{-1}) months after the end of salting could be the result of a slow release of salt from the overlying vadose zone. The second, early-summer peak could represent a pulse of salt from a source further upgradient. By October, the Cl^- had stabilized at approximately 1,000 mg L^{-1}. These observations support the assumptions made about the missing data from summer 2015.

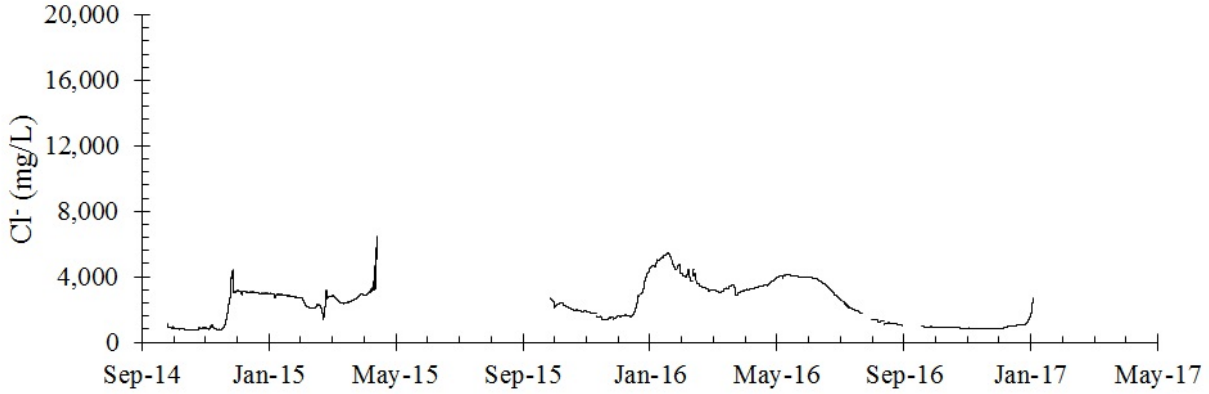

Figure 2.13: Cl^- concentration in well UG-1 during the period of study. Gaps in the record are present during probe failure, or when the probe was removed for cleaning or sampling.

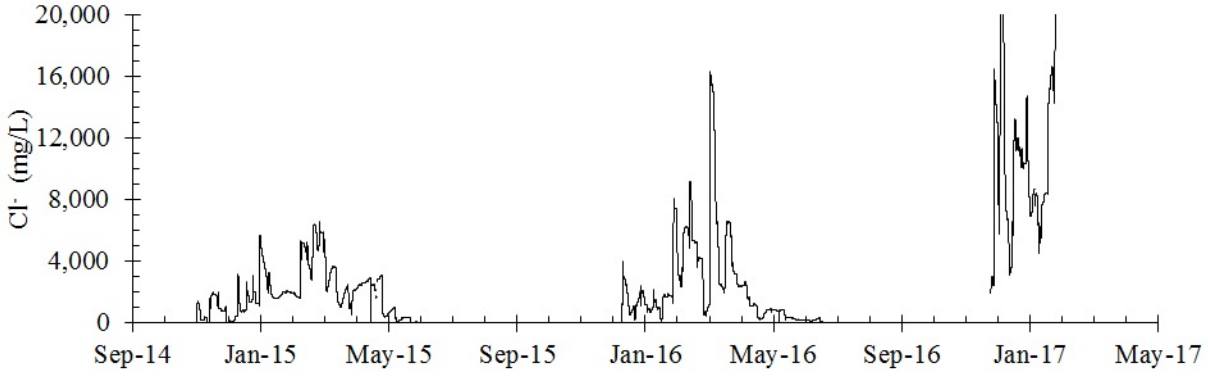

Figure 2.14: Cl^- concentration in well DG-1 during the period of study. Gaps in the record are present during probe failure, or when the probe was removed for cleaning or sampling.

DG-1

While the other wells were installed in thick glacial till of low hydraulic conductivity, this well is in a very sandy location, with a strong hydraulic connection to the parking lot, directly upgradient. Therefore, the Cl^- trend in this location is characterized by sharp spikes during the salting period. These pulses correspond to days of warm weather, when ice thaws following a salting event. In addition to these event-specific pulses, a seasonal trend can also be observed: a more general pulse of Cl^- begins at the onset of de-icing and reaches a maximum in March. At this point, de-icing begins to abate and more freshwater can dilute the pulse down to zero (i.e. below detection limit) by June. This trend was observed in both 2015 and 2016.

DG-2

At the beginning of monitoring in this well in fall 2014, the Cl^- concentration was 220 mg L^{-1}; by the end of winter 2015 the well experienced an increase, reaching a maximum of approximately 2,000 mg L^{-1} mid-summer. This 4-month lag between peak de-icing and the maximum Cl^- observation suggests that the recharge zone for this well is approximately 4 months distance upgradient. Angel (2015) measured a hydraulic conductivity of 2.63×10^{-4} cm s^{-1} in this location; at this rate the recharge zone is 1.5-3.0 m upgradient from the well. No data exist between November 2015 and March 2016 due to a probe failure. Monitoring ceased in October 2016 for this same reason.

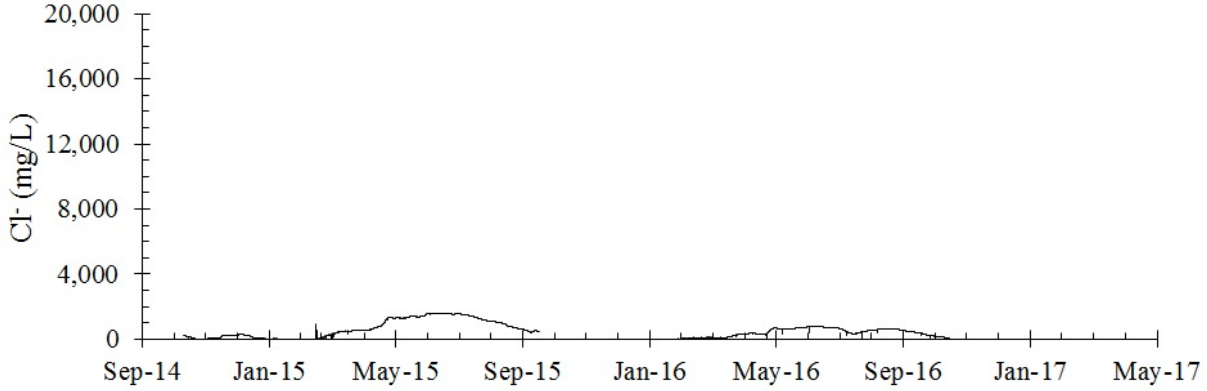

Figure 2.15: Cl^- concentration in well DG-2 during the period of study. Gaps in the record are present during probe failure, or when the probe was removed for cleaning or sampling.

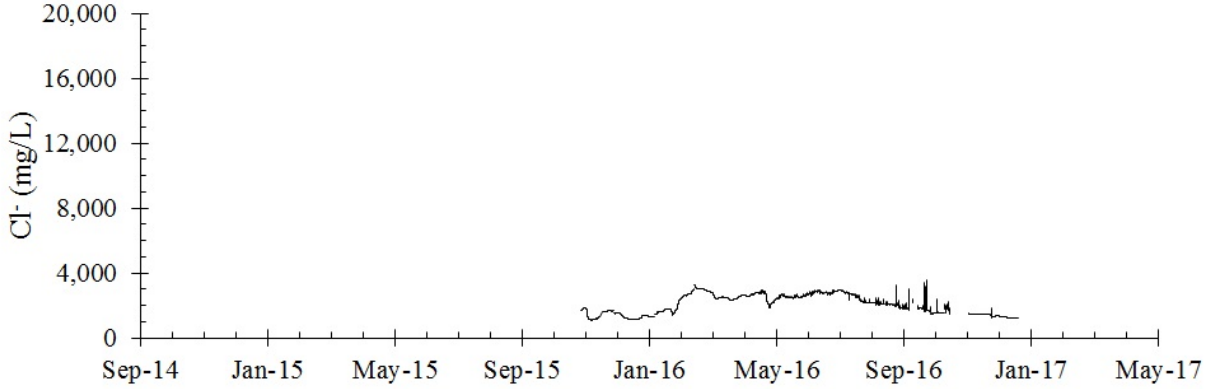

Figure 2.16: Cl^- concentration in well PZ-S during the period of study. Gaps in the record are present during probe failure, or when the probe was removed for cleaning or sampling.

PZ-S

The Cl^- trend in this well has higher variability than its neighbor, DG-3. This could be the result of the influence of multiple recharge zones, where fresh and saline water compete to form a more jagged trend. This trend could also be evidence for epikarst, or an overburden aquifer characterized by multiple hydraulic conductivities (Garcia-Fresca 2007). While conduits of higher K likely are present around the subterranean infrastructure at this site, they would have more muted influence in this location as the soil core consisted of thick clay and glacial till. Saline inputs from nearby sidewalks are more likely to be the explanation for these peaks in March and May.

The spikes observed in August-October 2016 should be treated with skepticism as the probe failed to give accurate readings during this period. The downward trend from July to November is likely a reasonable estimation of the groundwater chemistry during that time; the specific conductivity of this water was verified by a handheld conductivity meter to assess the sensor's error. The sensor was replaced in November 2016.

As the Cl - trend begins to taper in August, this was assumed to be the point at which inputs of freshwater exceeded inputs of saline water. The 5-month lag between this point and the abatement of de-icing activities suggests that the furthest principal input of salinity is 3.7-1.9m upgradient from the well.

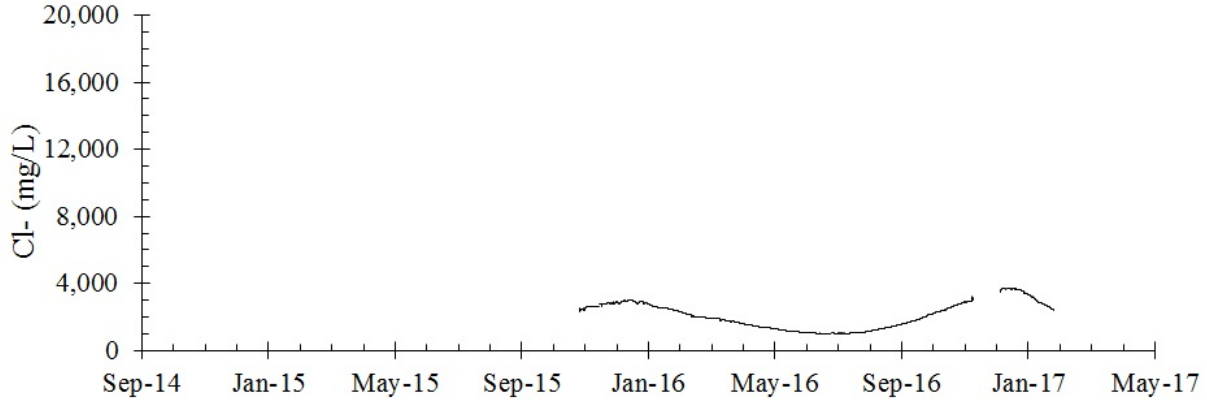

Figure 2.17: Cl^- concentration in well DG-3 during the period of study. Gaps in the record are present during probe failure, or when the probe was removed for cleaning or sampling.

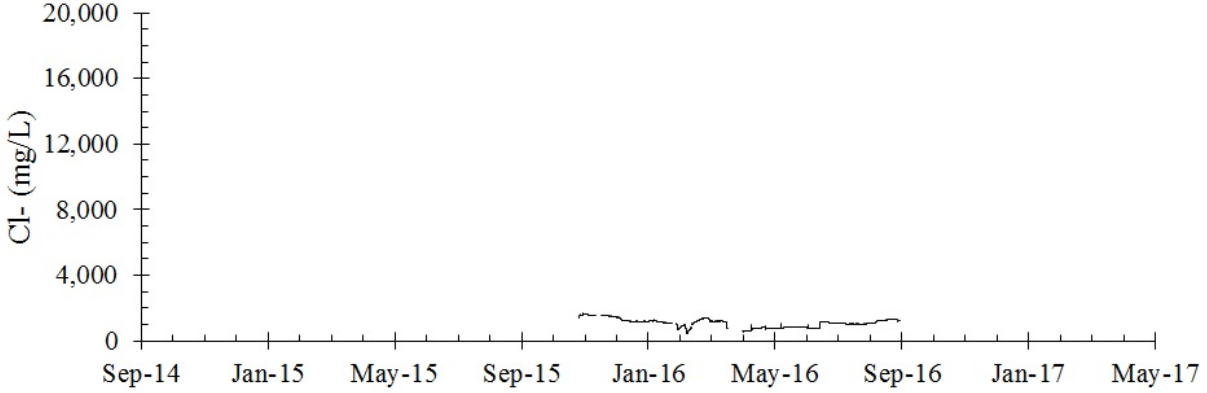

Figure 2.18: Cl^- concentration in well DG-4 during the period of study. Gaps in the record are present during probe failure, or when the probe was removed for cleaning or sampling.

DG-3

In mid-November 2015, a few weeks after installation, monitoring began in this well. An initial Cl^- concentration of 2,300 mg L^{-1} indicated that the groundwater in this area was also impacted by de-icing salt. Peak Cl^- is reached in this well during early January, after a gradual increase by 3,000 mg L^{-1} over 5 months. Given the hydraulic conductivity value for the site calculated by Angel (2015) and the ten-month lag between the well's maximum Cl^- observation and peak de-icing, the area of saline recharge is approximately 3.7-7.5 m upgradient from this well (i.e. at the extent of sandy fill beneath anthropogenic disturbances). Therefore, the peaks observed in early January represent de-icing applications from the previous winter.

DG-4

A record of the Cl^- concentration at this well exists for less than one year; monitoring began mid-November 2015 and ceased in mid-September 2016 due to probe failure. The well reached a minimum of 600 mg L^{-1} during early summer. The maximum Cl^- (1,600 mg L^{-1}) was observed in November 2015. The prevalence of elevated Cl^- throughout the year suggests the influence of slower, gradual saline inputs to groundwater at this location, such as salt slowly percolating down from the vadose zone.

Summary of Cl^- transport within the study area

The area is treated with de-icing salt between the months of November and April. Until March, the amount of saline meltwater typically exceeds the input of fresh rainwater. After this point, rainwater becomes the predominant input and the groundwater Cl^- begins to decrease. This annual 'pulse' is observed first in locations closer to recharge zones (i.e. well DG-1), and subsequently in locations further from recharge zones.

While the influence of the PA parking lot is apparent, additional, more subtle recharge zones adjacent to curbs and sidewalks provide a slower yet consistent input of salinity. This influence is observed in well UG-1, as high Cl^- (ca. 1,000 mg L^{-1}) is present as a background level (i.e. stable, non-winter concentration) with no input from the PA. Evidence of this

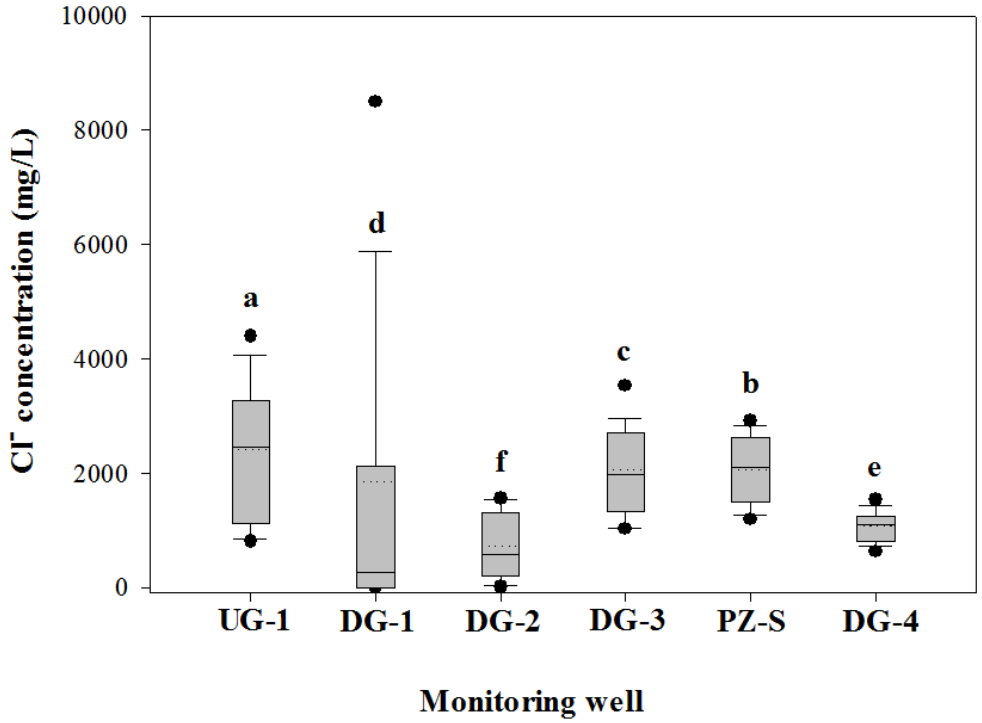

Figure 2.19: Box plots of all Cl^- data for each well. The median and mean Cl^- are represented by solid and dashed lines, respectively. The lower and upper black circles denote 5^{th} and 95^{th} percentiles. Wells with different letters are significantly different according to Tukey's HSD test, $\alpha = 0.05$. Mean separation was performed on a log-transformation of the data. Outliers are not plotted.

input is also seen in well PZ-S, where multiple recharge zones appear as multiple peaks in March, April and early August.

In order to further summarize the Cl^- data from the site, box plots were generated using the observations from each well (Figure 2.19). As these data did not follow a normal distribution, a log-transformation was performed prior to ANOVA mean separation testing.

Mean Cl^- is higher upgradient from the parking lot (UG-1) than it is in wells further downgradient (DG-3, PZ-S). Therefore, despite large inputs of salinity during winter months (as seen in the wide range of well DG-1), for most of the year fresh rainwater serves to dilute and lower these concentrations from the high background levels seen in UG-1. It is likely that this diluting effect would be greater if reduced de-icer application rates were used on the porous surface; the transportation-safety feasibility of this management strategy is

demonstrated in Roseen et al. (2012).

The long-term effect of permeable pavement on winter de-icing salt contamination of groundwater beneath permeable asphalt in areas without high background salinity is not known. However, in shallow urban aquifers such as the one in this study, the impact of de-icing salt is ubiquitous. Therefore it can be concluded that permeable asphalt can help reduce salinity in aquifers of high background salt concentration, which could have further benefits in reducing symptoms of urban stream syndrome. In non-urban (i.e. drinking water) aquifers, these inputs of salinity from stormwater infiltration practices may have detrimental water quality consequences.

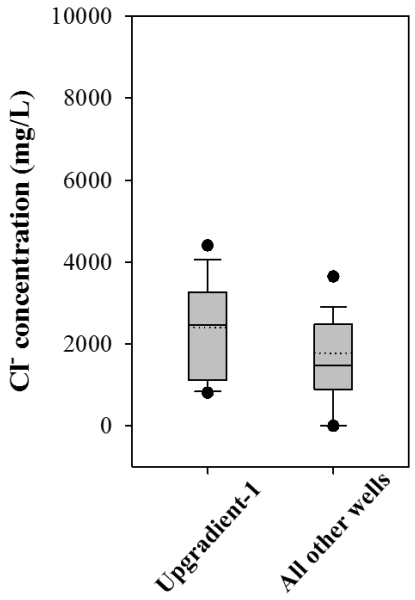

Figure 2.20: Box plots comparing Cl^- data from UG-1 with that of all other wells (DG-1 to 4, PZ-S). Means (dotted line) are significantly different based on a Satterthwaite 2-sample t-test ($p<0.0001$)

The effect of the pervious surface is further demonstrated in Figure 2.20, where the mean upgradient Cl^- concentration is significantly higher than that for all other wells.

2.3.4.2 Radionuclides

Water table elevations (WTE) and groundwater quality results from March 1 to March 3, 2016 are summarized in Table 2.5. The temperatures of the samples are listed in Table 2.6. Na^+, Ra and Rn data were used to generate concentration contour maps of the site (Figures 2.21a-c). The highest Na^+ concentrations measured were found directly downgradient of the parking lot (Figure 2.21a), indicating that high levels of salt reach the groundwater at the permeable pavement, then travel downgradient along the advective flow path shown in Figure 2.6. Correspondingly, high concentrations of Ra were found in locations with high Na^+ concentrations (Figures 2.21a,b). The significance of the correlation between the distributions

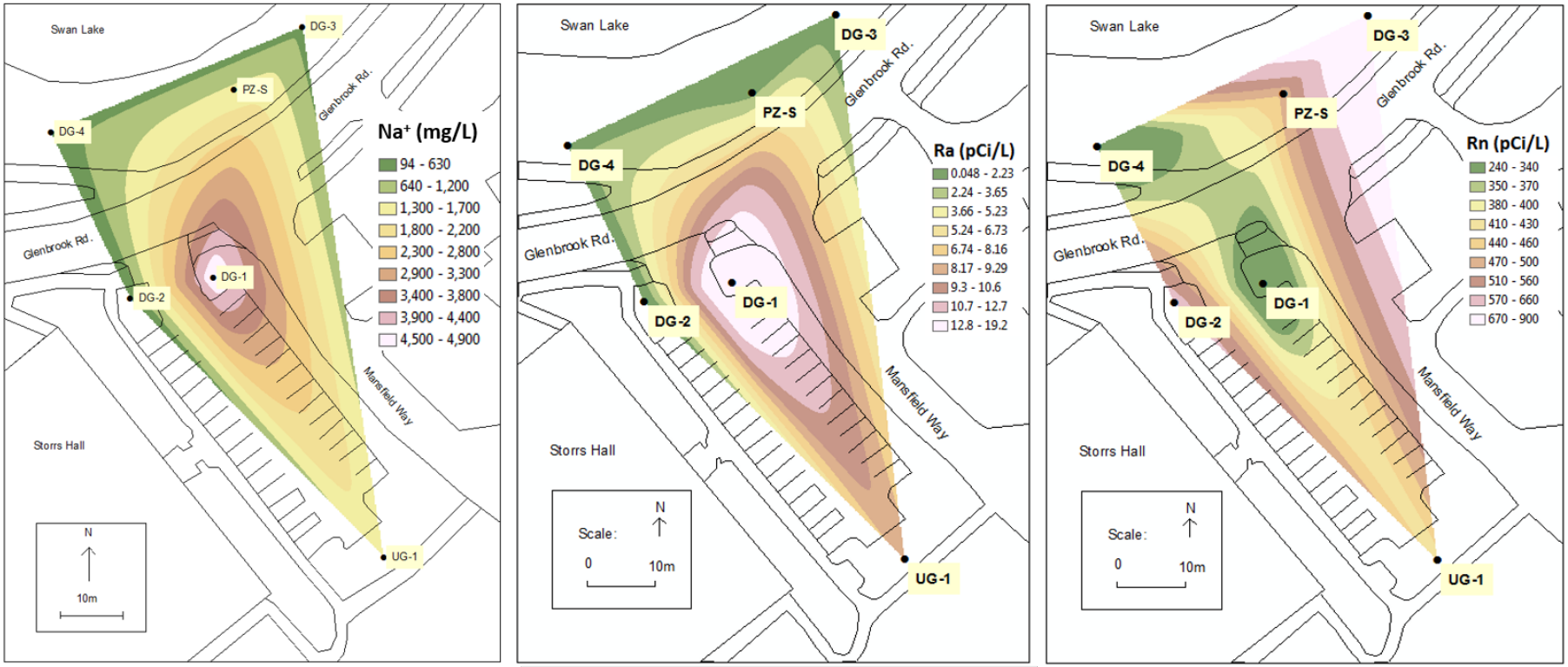

Figure 2.21: Spatial interpolations of (A) Na^+, (B) combined $^{226}Ra + ^{228}Ra$, and (C) ^{222}Rn. Concentration contours were generated in ArcMap using a natural neighbor algorithm.

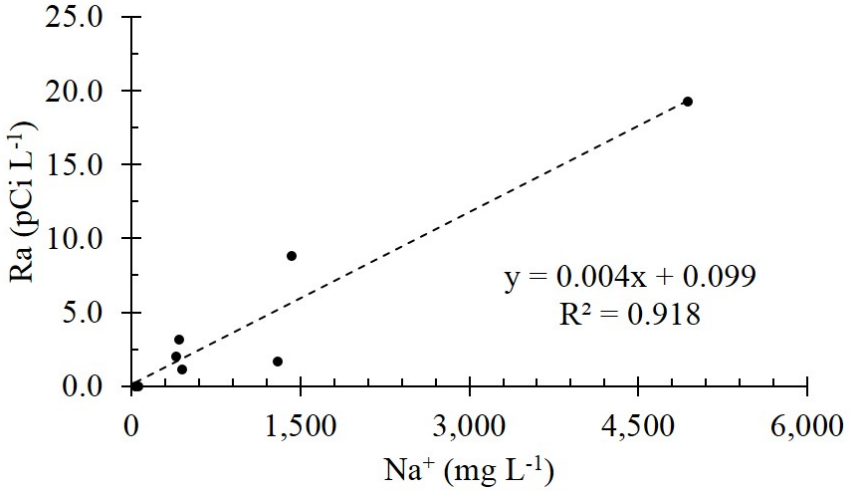

Figure 2.22: Positive correlation (p<0.001) between Ra activity and Na^+ concentration for groundwater samples.

of these elements was tested using ANOVA (IBM, 2012). A significant (p<0.001) positive linear correlation ($R^2 = 0.92$) between Ra and Na^+ concentrations was found (Figure 2.22). Ra was expressed as a combination of its most common isotopes (^{226}Ra and ^{228}Ra) to be consistent with regulatory units.

Table 2.5: Groundwater data from samples collected 1-3 March 2016 (Units of depth to water (DTW) and water table elevation (WTE) are in m, specific conductance (SC) values are μS cm^{-1}, units of common ions are mg/L, and units of radionuclides are pCi/L.).

Well ID	**DTW**	**WTE**	**SC**	**Na^+**	**Ca^{2+}**	**Mg^{2+}**	**Cl^-**	**^{222}Rn**	**Ra_{tot}**
UG-1	3.52	186.39	6250	1424.0	372.3	55.7	3944.5	417.0	8.78
DG-1	2.91	185.21	18300	4936.0	183.8	34.9	10899.0	242.0	19.26
DG-2	2.93	185.25	719	65.3	78.4	20.5	212.1	610.0	<2.00
DG-3	0.73	183.78	3787	450.6	397.0	117.7	2422.0	907.0	1.13
DG-4	3.51	183.45	3040	402.4	65.2	11.9	1825.3	*243.0	2.03
PZ-S	1.16	183.79	5520	1302.0	289.7	64.5	3417.0	470.0	1.66
PZ-D	1.14	183.81	3400	425.9	397.5	105.6	1946.0	979.0	3.14
WB-1	2.91	185.99	390	36.8	29.3	6.0	80.0	498.0	<2.00

*Questionable result due to gas loss by aeration during sampling

The spatial distribution of Rn at this site (Figure 2.21c) is characterized by a low point in the most saline well (DG-1) and relatively higher activities in surrounding, less saline wells. Low concentrations of Rn were also observed in well DG-4; this was likely due to gas loss during sampling. The Rn/salinity relationship ($R^2 = 0.61$) was less significant (p=0.059),

but negative (Figure 2.23), which was different from the significant positive relationship found for Ra/Na^+. Although eqn. 2.1 requires a mass concentration in the salinity term (i.e. TDS), specific conductivity was used in this plot as TDS values were not measured, but are linearly proportional to conductivity (Figure 2.5b). This model was used to predict the Henry's law constant, and subsequently the vapor-phase concentrations of Rn in equilibrium with the aqueous Rn measured in the samples.

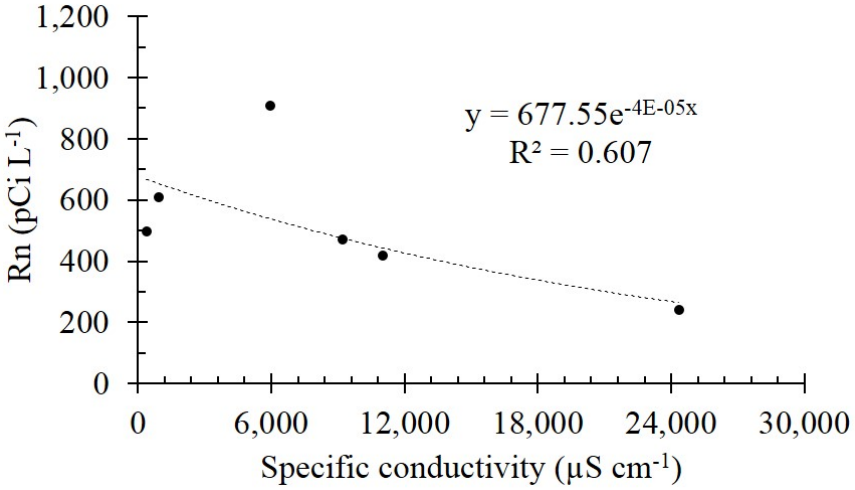

Figure 2.23: Negative exponential correlation (p=0.054) between aqueous Rn and conductivity (as a proxy for TDS), as described by eqn. 2.1. The Rn sample from well DG-4 was excluded from regression analysis.

Table 2.6: Predicted gaseous Rn concentrations based on aqueous Rn concentrations, temperature and salinity (TDS).

Location	**Rn_{aq} pCi L^{-1}**	***TDS g L^{-1}**	**Temp (°C)**	**K_H (dimensionless)**	**Rn_g pCi L^{-1}**
UG-1	417	5.80	11.96	0.313	1330
DG-1	242	16.05	21.60	0.221	1100
DG-2	610	0.38	22.14	0.233	2620
DG-3	907	3.39	10.57	0.333	2730
DG-4	**243	2.30	13.38	0.304	800
PZ-S	470	5.07	10.48	0.331	1420
PZ-D	979	2.88	10.48	0.336	2930
WB-1	498	0.15	14.90	0.292	1710

K_H: Ratio of liquid to gaseous concentration, values calculated from Schubert et al. 2012, eqn. 3a.
*Sum of known ion species (Na^+ Mg^{2+} Ca^{2+} and Cl^-)
**Radon gas loss likely during sampling due to limited amount of water in the well

Cation exchange is the primary process responsible for the presence of Ra in groundwater. The formation of $RaCl^+$ complexes also contributes to this (Sturchio et al. 2001, Tamamura et al. 2014). The high concentrations of Ra in some of the water samples were unexpected; two of the wells had Ra activities above the EPA drinking water standard of 5 pCi L^{-1} (UG-1: 8.78 pCi L^{-1}; DG-1: 19.26 pCi L^{-1}) (EPA 2000). Given the rare occurrence of Ra in groundwater (Hem 1985), the strong relationship found between Ra and Na^+ at this site indicates that groundwater contaminated with de-icing salt can release Ra from soil at levels nearly four times the regulatory limit. While the soil concentration of Ra was not measured, it can be assumed that the presence of detectable levels of Rn in all samples indicates a corresponding presence of a combination of solid- and liquid-phase Ra. The spatial extent of this Ra mobilization and the possibility of its occurrence in bedrock aquifers require further investigation.

Intuitively, an increase in aqueous Ra should be accompanied by an increase in its daughter nuclide: Rn. As discussed in the literature review, the emanation coefficient of Rn in rock is much lower than that in water. However given the volatility of this atom, this correlation was not observed clearly, indicating that the abundance of Rn groundwater is governed by a host of geochemical factors in addition to the supply of the parent nuclide.

As noted above, a weak inverse correlation was observed between specific conductivity and Rn in the groundwater (Figure 2.23). With all other factors held constant, the abundance of Rn in the aqueous phase would be expected to decrease logarithmically as a function of salinity, according to the Weiss equation (Eqn. 2.1). While this result somewhat demonstrates the 'salting out' phenomena quantified by Schubert et al. (2012), other physical factors (e.g. proximity of the well screen to the water table surface, temperature, permeability and moisture of unsaturated overburden soil) can have significant influence on the observed concentrations of Rn (Ball et al. 1991). Table 2.6 summarizes calculations of gaseous Rn concentrations that would be in equilibrium (i.e. in the vadose zone directly above the water table) with the observed aqueous Rn concentrations. The K_H values were

adjusted for salinity according to the model developed by Schubert et al. (2012), using groundwater temperatures measured during the collection of aqueous samples. In every case, the equilibrium Rn gas concentration far exceeds the 4 pCi/L EPA indoor air quality standard (EPA 1986). Additionally, wells DG-1 and DG-2 are in very close proximity to a steam line; this common feature of urban subsurface geology doubles the groundwater temperature. These higher temperatures substantially decrease the K_H of Rn, further enhancing Rn volatilization to the vadose zone. While the theoretical vapor-phase Rn concentrations did exceed the air quality standard, substantial dispersion is expected to occur between the piezometric and ground surfaces. Measurements of gaseous Rn at (or near) the ground surface would be more robust descriptors of the behavior of carcinogenic (i.e. inhalable) Rn.

Rn was found in the background water sample from well WB-1. However, Ra, its parent isotope, was not detected. The water also had a low Na^+ concentration. Given that the K_H of Ra is typically very high in non-saline conditions, the Ra source must be in the solid phases of either the till or the underlying bedrock.

2.3.4.3 Metal cations

The concentrations of major cations (Na^+,Ca^{2+},Mg^{2+}) were measured by Angel (2015) to assess their relative abundance under salting and non-salting conditions. These data were compared with that of samples from the following year (Figure 2.24). The relative concentration of each cation did increase from 2015 to 2016, but values were within an order-of-magnitude. This relative consistency suggests that the salt input does not vary greatly from year to year. Surprisingly, this slight increase was observed even though winter 2015 experienced greater snowfall than winter 2016. Assuming consistent de-icing practices, this increase could be evidence for an annual accumulation of cations. To demonstrate that active cation exchange is taking place, Figure 2.25 was plotted: a comparison between Na^+ and Cl^-. While there is a strong correlation between moles of salt-derived Na^+ and Cl^-,

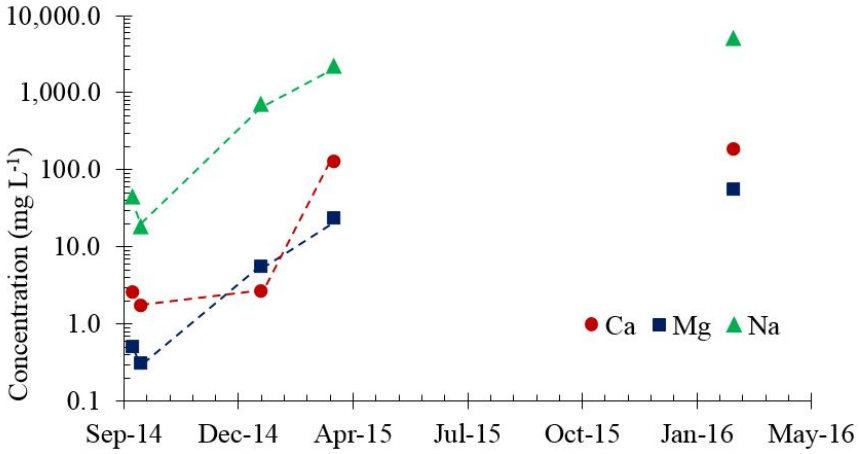

Figure 2.24: Concentrations of major cations in groundwater samples for well DG-1.

the slope is less than one, indicating a deficit of Na^+. The occurrence of cation exchange is supported by relatively high levels of dissolved Ca^{2+} and Mg^{2+} at the permeable pavement study area compared to those of the background well WB-1 (Table 2.5).

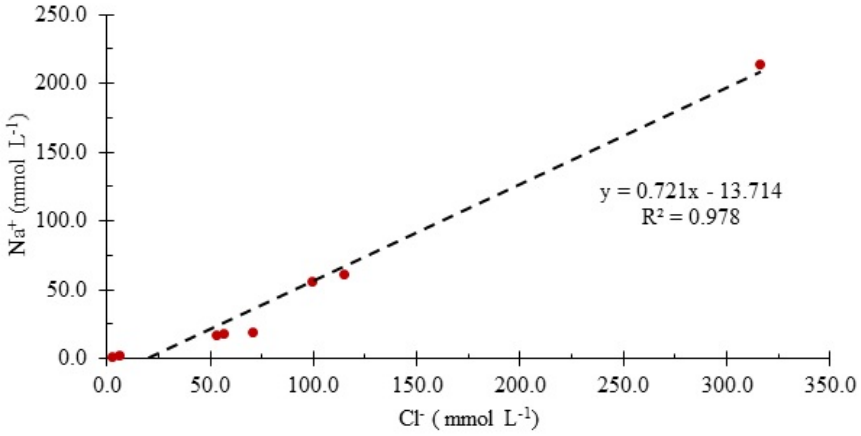

Figure 2.25: Molar comparison of Na^+ and Cl^- ions. Note that the slope of the linear regression is 0.72, indicating a deficiency of Na^+ relative to Cl^-

Despite the water sample from well DG-1 having the highest specific conductivity, its relative Ca^{2+} and Mg^{2+} content were not as high as other wells (Table 2.5). Spatially, the distributions of these divalent cations are not identical to that of Na^+, which further supports the conclusion that Na^+ is the primary cationic component of de-icing salt. The

distributions of Ca^{2+} and Mg^{2+} suggest that these cations accumulate in areas of perennially high salinity, such as UG-1, DG-3, and PZ-S. Sampling during non-salting months at the study area could help further assess this conclusion.

2.3.4.4 Vertical variation

As described in Table 2.1, wells PZ-S and PZ-D extend to depths of 2.13 and 3.96 m below grade, respectively. A contrast can be seen between the chemistry of the water samples taken from these two wells. The specific conductivity of PZ-S was nearly double that of PZ-D, which suggests that a lens of more saline water overlies older, fresh water. However, the conductivity of PZ-D is an order of magnitude greater than background levels; this demonstrates that any interface between a saline lens and underlying freshwater is not sharply defined, but instead exists as a gradient.

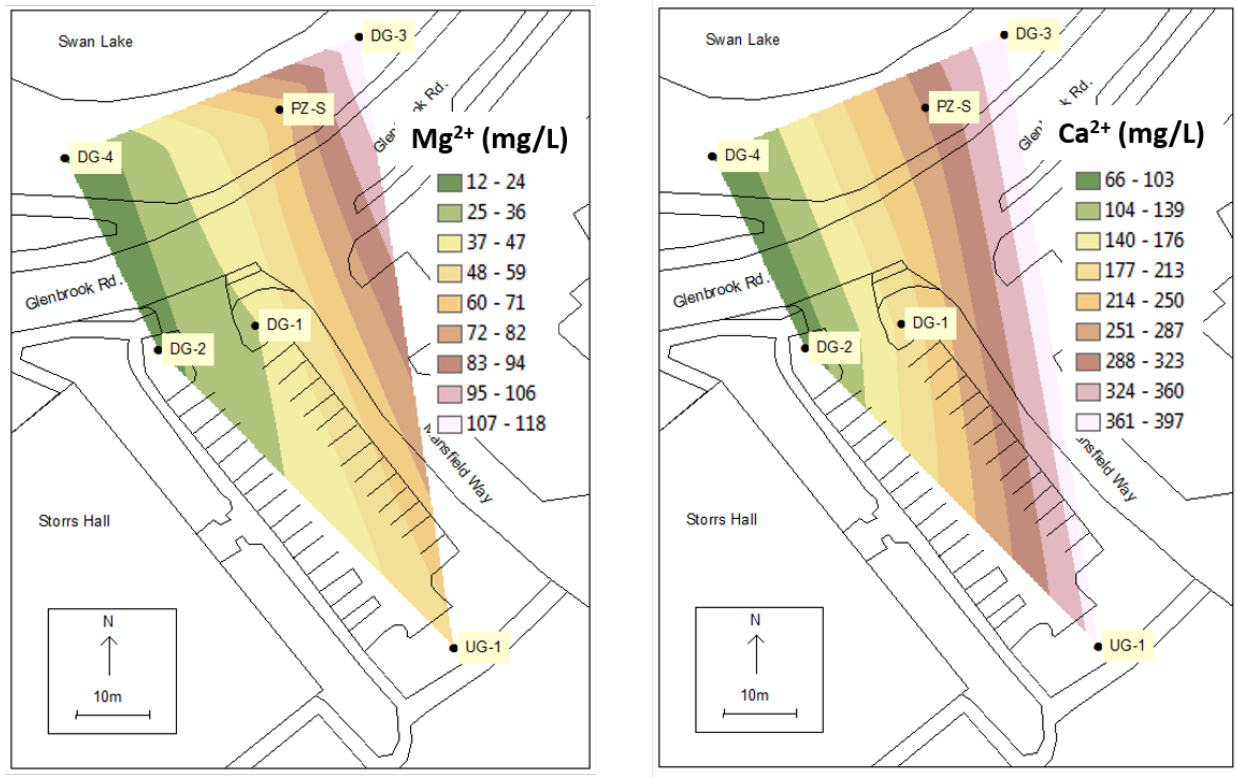

Figure 2.26: Spatial distributions of Mg^{2+} (left) and Ca^{2+} (right) dissolved ion concentrations in groundwater samples. Contour surfaces were generated using a natural neighbor interpolation algorithm.

In addition to the total salinity, the relative ionic composition also varies with depth. Na^+ is the dominant cation in the upper aquifer, with Na^+/Ca^{2+} and Na^+/Mg^{2+} ratios of 4.5 and 20.2, respectively. In PZ-D, much lower Na^+/Ca^{2+} and Na^+/Mg^{2+} ratios occur: 1.1 and 4.0, respectively. On a molar equivalence basis, Na^+ outnumbers $Ca^{2+} + Mg^{2+}$ by 36.9 meq L^{-1} in PZ-S, but in PZ-D the divalent cations outnumber Na^+ by 10.0 meq L^{-1}. This suggests that Na^+ preferentially adsorbs to the weathered till at this site.

While it is possible that the background hardness increases with depth at this location, it is likely that there is a longer flow path between this deeper well and its respective recharge zone. Therefore, the chemical evolution of this water is more developed, that is, more cation exchange has occurred in PZ-D than in its shallower counterpart. Metcalf and Robbins (2013) describe this process as a buffering of Na^+ in groundwater. These possibilities could be further assessed with a tracer test, isotopic analysis, or a long-term conductivity probe.

2.4 Conclusion

Groundwater at this study area is highly impacted by inputs of de-icing salt during winter. Multiple peaks in long-term Cl^- trends suggest that salt inputs come from multiple sources. The persistence of Cl^- at concentrations greater than 1000 mg L^{-1} throughout the year in well UG-1 reinforces previous conclusions about the primary importance of sidewalks as a source (Angel 2015; Dietz et al. 2016). In downgradient wells, de-icing salts persist in the soil and groundwater throughout the year despite substantial dilution by rainwater during non-winter months. Further monitoring is necessary to quantify the rate of salt accumulation at this site, but data from nearly two years of monitoring demonstrate that yearly minimum salinity values are increasing. This corresponds with similar trends observed in the water of other snow-affected regions.

The anthropogenic salinity observed at this site can serve to release soil-bound Ra atoms to the groundwater at levels exceeding federal drinking water standards. This is the first identification of this phenomena, so the spatial extent of its occurrence must be further inves-

tigated. Additionally, this mobilization should be assessed in bedrock aquifers to evaluate the risk of Ra contamination in drinking water. Evidence was presented for the salting-out of Rn from the water table, however subsequent samples should be collected during non-winter months to assess the seasonal variability of aqueous Rn concentrations. The Henry's law calculations suggest that buildings adjacent to or downgradient from (a) highly permeable locations that are deiced with salt or (b) locations with elevated subsurface temperature could be periodically subjected to high Rn diffusive fluxes. The degree of increased radionuclide exposure would depend on a number of key site-specific factors including direction of groundwater flow, location of dwellings, water temperature, depth to groundwater and soil properties influencing gas migration. The potential public health implication of these findings is strong justification for further study of this phenomenon.

Although our study focused on an area of permeable pavement, the results would be equally applicable to any salted location where there is a high infiltration rate to groundwater, such as an urban riparian floodplain (Ledford et al. 2016). Therefore, de-icing activity should be closely monitored or reduced near these areas of higher potential for groundwater contamination.

2.5 References

Agency for Toxic Substances and Disease Registry (ATSDR) (1990) Toxicological profile for radium. Atlanta, GA: U.S. Department of Health and Human Services, Public Health Service.

Angel, D. (2015) Effects of winter de-icing on groundwater quality beneath permeable asphalt. Master's thesis, University of Connecticut.

Arnold, C.L., Gibbons, C.J. (1996) Impervious surface coverage: the emergence of a key environmental indicator. *Journal of the American Planning Association.* **62(2)**, 243-258.

Arnold, C.L. (2011) Responding to an impervious cover-based TMDL: a brief step-by-step guide. Center for Land Use Education and Research (CLEAR). Publication 110830.1.

Asplund, G., Grimvall A. (1991) Organohalogens in nature: more widespread than previously assumed *Environ. Sci. Technol.* **25(8)** 1346-1350.

Bäckström, M., Karlsson, S., Bäckman, L., Folkeson, L. and Lind, B. (2004) Mobilisation of heavy metals by de- icing salts in a roadside environment. *Water Research* **38,** 720-732.

Bastviken, D., Thomsen, F., Svennson, T., Karlsson, S., Sandén, P., Shaw, G., Matucha, M., Öberg, G. (2007) Chloride retention in forest soil by microbial uptake and by natural chlorination of organic matter. *Geochimica et Cosmochimica Acta* **71,** 3182-3192.

Belitz, K., Jurgens, B.C., Johnson, T.D. 2016. Potential corrosivity of untreated groundwater in the United States. U.S. Geological Survey Scientific Investigations Report 2016-5092.

Borst, M., Brown, R.A. (2014) Chloride released from three permeable pavement surfaces after winter salt application. *Journal of the American Water Resources Association* **50(1)** 29-41.

Boving, T., Stolt, M., Augenstern, J., Brosnan, B. (2008) Potential for localized groundwater contamination in a porous pavement parking lot setting in Rhode Island. *Environ. Geol.* **55** 571-582.

Brady, S. (2012) Road to evolution? Local adaptation to road adjacency in an amphibian (Ambystoma maculatum). *Nature: Scientific Reports* **2**, article no. 235.

Brown, C., Mullaney, J., Morrison, J., Martin, J., Trombley, T. (2015) Chloride concentrations, loads, and yields in four watersheds along interstate 95, Southeastern Connecticut, 2008–11 — factors that affect peak chloride concentrations during winter storms. U.S.

Geological Survey Scientific Investigations Report 2015–5057, 68 p

Bubeck, R.C., Diment, W.H., Deck, B.L., Baldwin, A.L., and Lipton, S.D. (1971) Runoff of de-icing salt: effect on Irondequoit Bay, Rochester, New York. *Science* **172(3988)** 1128-1132.

Calabrese, E.J., Tuthill, R.W. (1978) Sources of elevated sodium levels in drinking waer and recommendations for reduction. *Journal of Environmental Health* **41(3)**, 151-155.

Cassanelli, J.P., Robbins, G.A. (2013) Effects of road salt on Connecticut's groundwater: a statewide centennial perspective. *J. Envion. Qual.* **42,** 737-748.

Chow, V.T., Maidment, D.R., Mays, L.W. (1988) Applied Hydrology. Chapter 15, p. 498. McGraw Hill, New York.

Corsi, S.R., De Cicco, L.A., Lutz, M.A., and Hirsch, R.M. (2015) River chloride trends in snow-affected urban watersheds: increasing concentrations outpace urban growth rate and are common among all seasons. *Science of the Total Environment. 508,* 488-497.

CT DOT. (2013) Snow and Ice Guidelines. Office of maintenance, Connecticut Department of Transportation. CT DOT. (2015) An overview of snow and ice control operations on state highways in Conecticut. Connecticut Department of Transportation, Bureau of Highway Operations, Office of Maintenance, Newington, CT.

Darby, S.; Hill, D.; Doll, R. (2001) Radon: a likely carcinogen at all exposures. *Ann. Oncol.* **12(10)** 1341-1351.

Dennis, H.W. (1973) Salt pollution of a shallow aquifer – Indianapolis, Indiana. *Ground Water* **11(4)** 18-22.

Dietz, M.E. (2007) Low impact development practices: a review of current research and recommendations for future directions. *Water Air Soil Pollut.* **186,** 351-363.

Dietz, M.E. Angel, D.R., Robbins, G.A., McNaboe, L.A. (2016) Permeable asphalt: a new tool to reduce road salt contamination of groundwater in urban areas. *Groundwater* doi: 10.1111/gwat.12454

Garcia-Fresca, B. (2007) Urban-enhanced groundwater recharge: review and case study of Austin, Texas, USA. IAH Selected Papers on Hydrogeology 8. Ed. Howard, K. 3-18.

Goldman, C.R. and Horne, A.J. (1983) Limnology. McGraw-Hill Book Co., New York.

Hagemann, M. (2011) Molecular biology of cyanobacterial salt acclimation. *FEMS Microbiology Reviews* **35** 87- 123.

Hem, J.D. (1985) Study and interpretation of the chemical characteristics of natural water, third edition. U.S. Geological Survey Water Supply Paper 2254. Alexandria, VA.

Hirao, S.; Yamazawa, H.; Moriizumi, J. (2010) Estimation of the global 222 Rn flux density from the earth's surface. *Jpn. J. Health Phys.* **45(2)** 161-171.

Hood, M.J., Clausen, J.C., Warner, G.S. (2007) Comparison of stormwater lag times for low impact and traditional residential development. *Journal of the American Water Resources Association.* **43(4)** 1036-1046.

Hopfensberger, K., Burgin, A., Schopfer, V., and Helton, A. (2014) Impacts of saltwater incursion on plant communities, anaerobic microbial metabolism, and resulting relationships in a restored freshwater wetland. *Ecosystems* **17(5)** 792-807.

IAEA (2014) The Environmental Behaviour of Radium: Revised Edition. Technical Reports Series no. 476. International Atomic Energy Agency. Vienna.

Kaushal, S.S., Groffman, P.M., Likens, G.E., Belt, K.T., Stack, W.P., Kelly, V.R., Band, L.E., Fisher, G.T. (2005). Increased salinization of fresh water in the northeastern United States. *Proceedings of the National Academy of Sciences,* **102(38)**, 13517-13520.

Kelly, V.R., Lovett, G.M., Weathers, K.C., Findlay, S.E.G., Strayer, D.L., Burns, D.J., Likens, G.E. (2008). Long-term sodium chloride retention in a rural watershed: Legacy effects of road salt on streamwater concentration. *Environ. Sci. Technol.* **42** 410-415.

Kraemer, T., Reid, D. (1984) The occurrence and behavior of radium in saline formation water of the U.S. Gulf Coast region. *Chemical Geology* **46(2)** 153-174.

Kumar, A., Karpe, r., rout, S., Gautam, Y., Mishra, M., Ravi, P., Tripathi, R. (2016) Activity ratios of $^{234}U/^{238}U$ and $^{226}Ra/^{228}Ra$ for transport mechanisms of elevated uranium in alluvial aquifers of groundwater in southwestern (SW) Punjab, India. *Journal of Environmental Radioactivity* **151** 311-320.

Langmuir, D., Riese, A.C. (1985). The thermodynamic properties of Ra. *Geochim. et Cosmochim. Acta* **49(7)**, 1593-1601.

Larsen, H. (1986) Halophilic and halotolerant microorganisms – an overview and historical perspective. *FEMS Microbiology Reviews* **39** 3-7.

Lebo, S., Gargulak, J., McNally, T. (2001) Lignin. Kirk-Othmer Encyclopedia of Chemical Technology. DOI: 10.1002/0471238961.12090714120914.a01.pub2

Likens, G.E., Buso, D.C. (2010) Salinization of Mirror Lake by road salt. *Water Air Soil Pollution* **205** 205-214.

Mahoney, J., Jackson, E., Larsen, D., Vadas, T., Wille, K. and Zinke, S. (2015) Winter Highway Maintenance Operations: Connecticut. Connecticut Academy of Science and Engineering. CTDOT Publication CT-2289-F-15-1. Rocky Hill, CT.

Meriano, M., Eyles, N. and Howard, K. (2009) Hydrogeological impacts of road salt from Canada's busiest highway on a Lake Ontario watershed (Frenchman's Bay) and lagoon, City of Pickering. *Journal of Contaminant Hydrology* **107(1-2)**, 66-81.

Mullaney, J.R., Lorenz, D.L., Arnston, A.D. (2009) Chloride in groundwater and surface water in areas underlain by the glacial aquifer system, northern United States. U.S. Geological Survey Scientific Investigations Report 2009- 5086, 41p.

National Research Council. (2008) Urban Stormwater Management in the United States. National Academy of Sciences, National Academies Press, Washington, DC.

Nazaroff, W.W. (1992) Radon transport from soil to air. *Reviews of Geophysics* **30(2)** 137-160.

Nguyen, C.K.; Stone, K.R.; Edwards, M.A. 2011. Impact of chloride:sulfate mass ratio (CSMR) changes on lead leaching. *Journal American Water Works Association* **103**, 81-92.

Norrström, A., Jacks, G. (1998) Concentration and fractionation of heavy metals in roadside soils receiving de-icing salts. Science of the Total Environment 218, 161-174. Norrström, A. (2005) Metal mobility by de-icing salt from an infiltration trench for highway runoff. *Applied Geochemistry* **20**, 1907-1919.

Novotny E.V., Sander A.R., Mohseni O., Stefan H.G. (2009) Chloride ion transport and mass balance in a metropolitan area using road salt. *Water Resources Research* **45** W12410.

Öberg, G. (1998) Chlorid und organisch gebundenes Chlor in Böden. *Acta hydrochim. hydrobiol.* **26(3)** 137-144.

Pagotto, C., Legret, M., Le Cloirec, P. (2000) Comparison of the hydraulic behavior and the quality of highway runoff water according to the type of pavement. *Water Research* **34(18)** 4446-4454.

Perera, N., Gharabaghi, B. and Howard, K. (2013) Groundwater chloride response in the Highland Creek watershed due to road salt application: a re-assessment after 20 years. *Journal of Hydrology* **479**, 159-168.

Pitt, R., Clark, S., Field, R. (1999) Groundwater contamination potential from stormwater infiltration practices. *Urban Water* **1**, 217-236.

Prince George's County. (1999) Low-impact design strategies: an integrated design ap-

proach. Prince George's County, MD Department of Environmental Resources, Watershed Protection Branch, Landover, MD.

Robertson, A.; Allen, J.; Laney, R.; Curnow, A. (2013) The cellular and molecular carcinogenic effects of radon exposure: a review. *Int. J. Mol. Sci.* **14(7)** 14024-14063.

Roseen R.M., Ballestero, T.P., Houle, J.J., Briggs, J.F., Houle, K.M. (2012) Water quality and hydrologic performance of a porous asphalt pavement as a storm-water treatment strategy in a cold climate. *Journal of Environmental Engineering* **138** 81-89.

Sakoda, A.; Ishimori, Y.; Yamaoka, K. (2011) A comprehensive review of radon emanation measurements for mineral, rock, soil, mill tailing and fly ash. *Applied Radiation and Isotopes* **69(10)** 1422-1435.

Sanders, C.L. (2010) Radiation Hormesis and the Linear-No-Threshold Assumption. Korea Advanced Institute of Science and Technology, Springer, New York.

Schalk, C. and Stasulis, N. (2007) Relations among water levels, specific conductance and depths of bedrock fractures in four road-salt contaminated wells in Maine, 2007-9. US Geological Survey Scientific Investigations Report 2012-5205.

Schery, S.D.; Huang, S. (2004) An estimate of the global distribution of radon emissions from the ocean. *Geophysical Research Letters.* **31(19)** L19104.

Siegel, L. (2007) Hazard Identification for Human and Ecological Effects of Sodium Chloride Road Salt. New Hampshire Department of Environmental Services. http://www.rebuildingi93.com/documents/environmental/Chloride%20TMDL%20Toxicological%20Evaluation.pdf

Singh, S.; Jain, A.K.; Tuli, J.K. (2011) Nuclear data sheets for A = 222. *Nuclear Data Sheets* **112(11)** 2851-2886.

Sonmez, S., Buyutkas, D., Okturen, F., Citak, S. (2008) Assessment of different soil to water ratios (1:1, 1:2.5, 1:5) in soil salinity studies. *Geoderma* **144**, 361-369.

Sun, H., Alexander, J. Grove, B., and Koch, M. (2015) Mobilization of arsenic, lead, and mercury under conditions of sea water intrusion and road de-icing salt application. *Journal of Contaminant Hydrology* **180**, 12-24.

Szabo, Z., dePaul, V., Fischer, J., Kraemer, T. and Jacobsen, E. (2012). Occurrence and geochemistry of radium in water from principal drinking-water aquifer systems of the United States. *Applied Geochemistry* **27**, 729-752.

Tamaramura, S.; Takada, T.; Tomita, J.; Nagao, S.; Fukushi, K.; Yamamoto, M. 2014. Salinity dependence of 226 Ra adsorption on montmorillonite and kaolinite. *J Radioanal Nucl Chem.* **299,** 569-575.

Transportation Research Board (1991) Highway de-icing: comparing salt and calcium magnesium acetate. Special report 235. Committee on the Comparative Costs of Rock Salt and Calcium Magnesium Acetate (CMA) for Highway De-icing. Transportation Research Board, National Research Council, Washington, D.C.

US EPA. (1986) Quality Criteria for Water. EPA-440/5-8-001; USEPA Office of Water Regulations and Standards. Washington, DC

US EPA. (2000) National Primary Drinking Water Regulations; Radionuclides; Notice of Data Availability; Proposed Rule. *Federal Register* **65(78)** 21575-21628.

USGS. (1940-2016) Minerals Yearbook: Salt. USGS Mineral Resources Program. Reston, VA.

Walsh, C.J., Roy, A.H., Feminella, J.W., Cottingham, P.D., Groffman, P.M., Morgan, R.P. (2005) The urban stream syndrome: current knowledge and the search for a cure. *J. N. Am. Benthol. Soc.* **24(3)** 706-723.

Weiss, R.F. (1970) The solubility of nitrogen, oxygen and argon in water and seawater. *Deep-Sea Research* **17(4)** 721-735.

Wilkening, M.H., Clements, W.E., Stanley, D. (1972). Radon 222 flux measurements in widely separated regions (CONF-720805–P2). Gesell, T.F. (Ed.). United States

Wetzel, R.G. (1975) Limnology. W.B. Saunders Co., Philadelphia, PA.

World Health Organization (WHO) (1979). Sodium, chlorides and conductivity in drinking water. EURO Reports and Studies no. 2 Copenhagen, WHO Regional office for Europe.

Wood, W., Kraemer, T., Shapiro, A. (2004) Radon (^{222}Rn) in ground water of fractured rocks: a diffusion/ion exchange model. *Ground Water* **42(4)** 552-567.

Yan, N., Marschner, P., Cao, W., Zuo, C., Qin, W., (2015) Influence of salinity and water content on soil microorganisms. *International Soil and Water Conservation Research* **3(4)** 316-323.

Appendices

Appendix A

Boring logs

Soil boring logs for wells DG-3, DG-4, PZ-S, PZ-M and PZ-D are included in this appendix. For the boring logs of wells UG-1, DG-1 and DG-2, refer to appendix A in Angel (2015). This record uses a non-abbreviated well nomenclature; the wells are named Upgradient, Downgradient 1, and Downgradient 2, respectively.

University of Connecticut
Dept. of Natural Resources
Lukas McNaboe

Log of Boring: DG-3

Easternmost downgradient well, located North of Glenbrook Road, approximately 15 feet from the park bench and approximately 25 feet from the sidewalk.

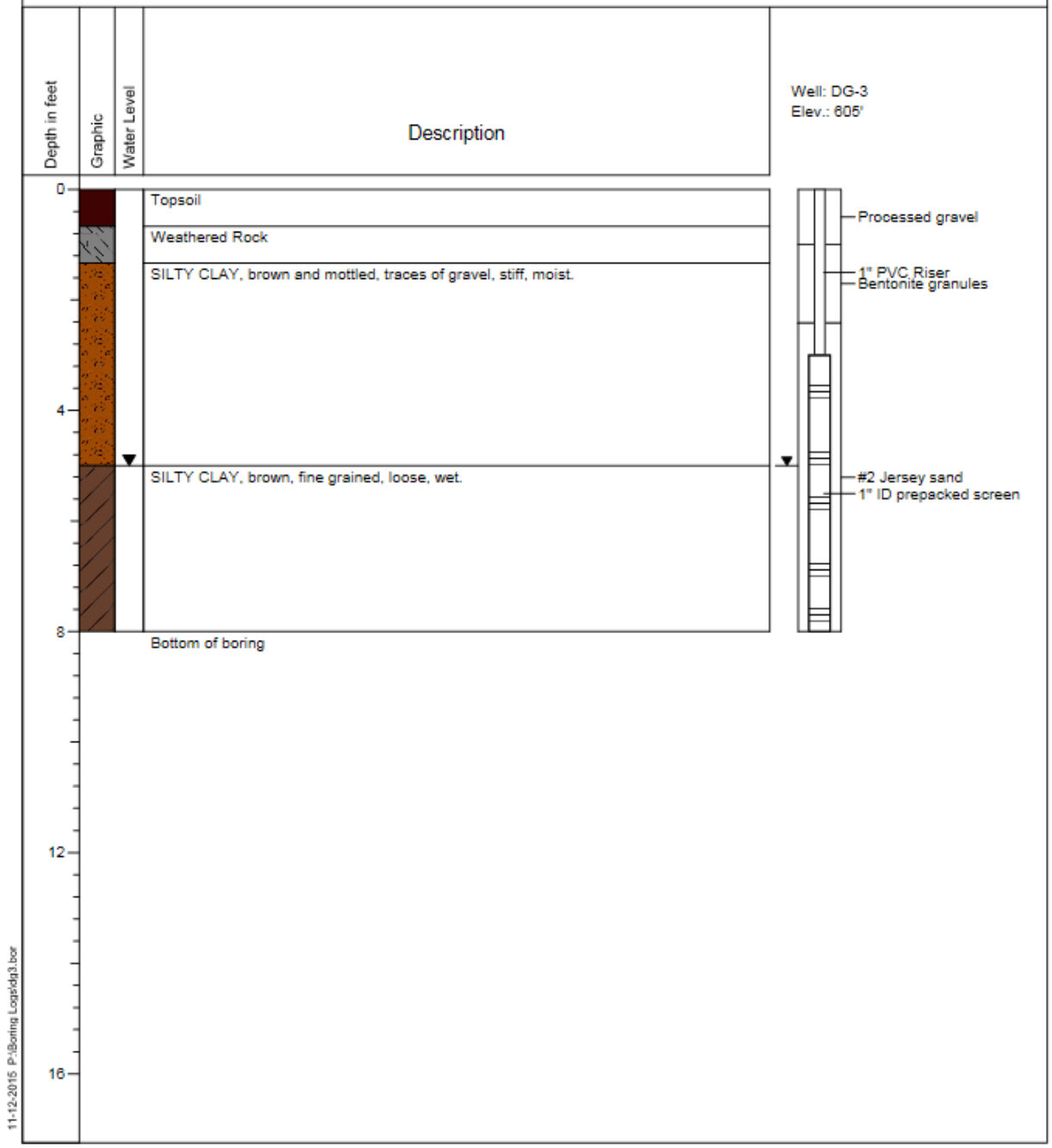

University of Connecticut
Dept. of Natural Resources
Lukas McNaboe

Log of Boring: DG-4

Westernmost downgradient well, located North of Glenbrook Road, slightly West of both crosswalks, approximately 7 feet from the sidewalk.

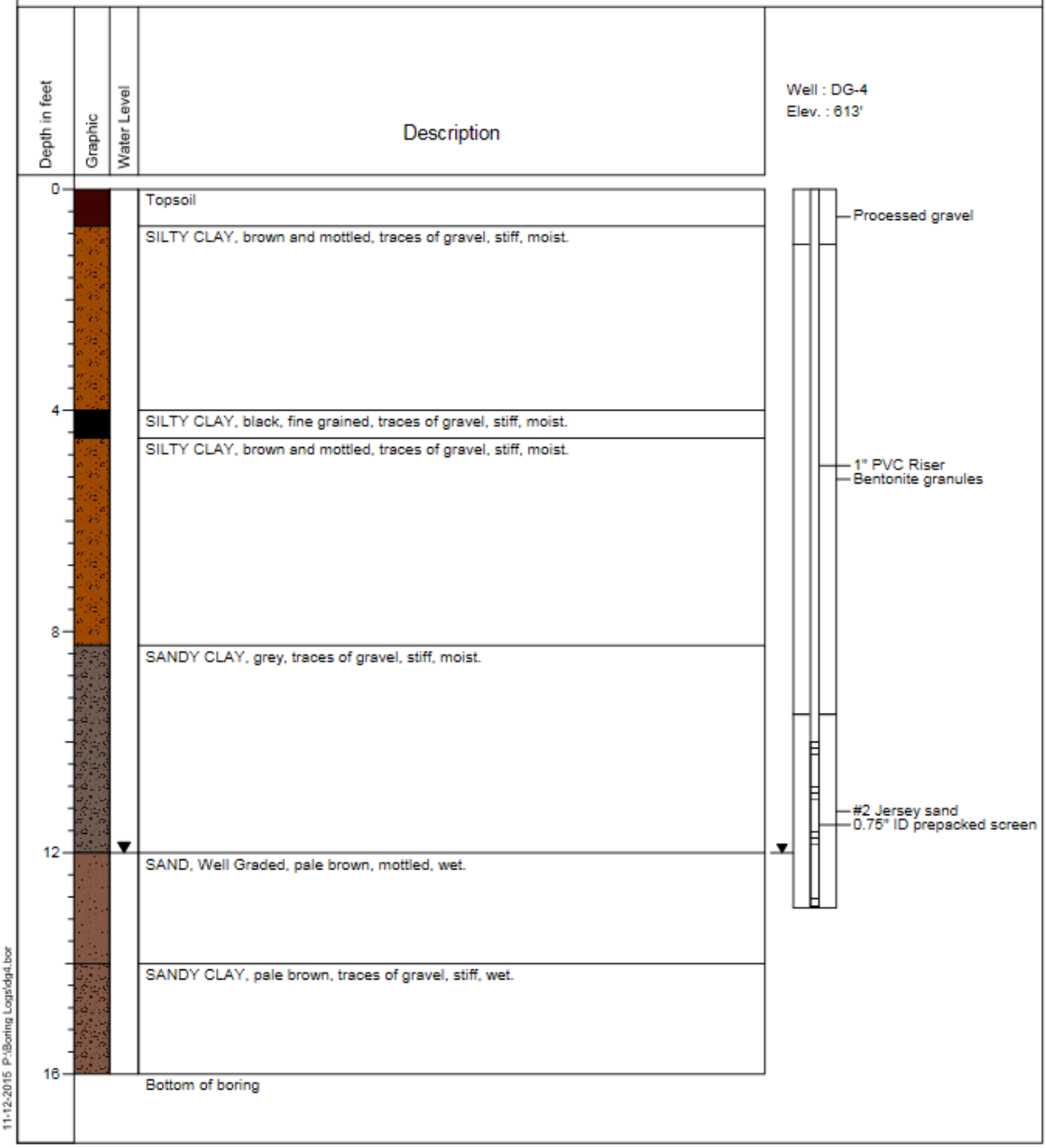

University of Connecticut
Dept. of Natural Resources
Lukas McNaboe

Log of Boring: PZ-S

Clustered Piezometer:
Shallowest of 3 monitoring wells, installed well depth of 7', located North of Glenbrook Road, slightly East of both crosswalks, approximately 20 feet from the sidewalk.

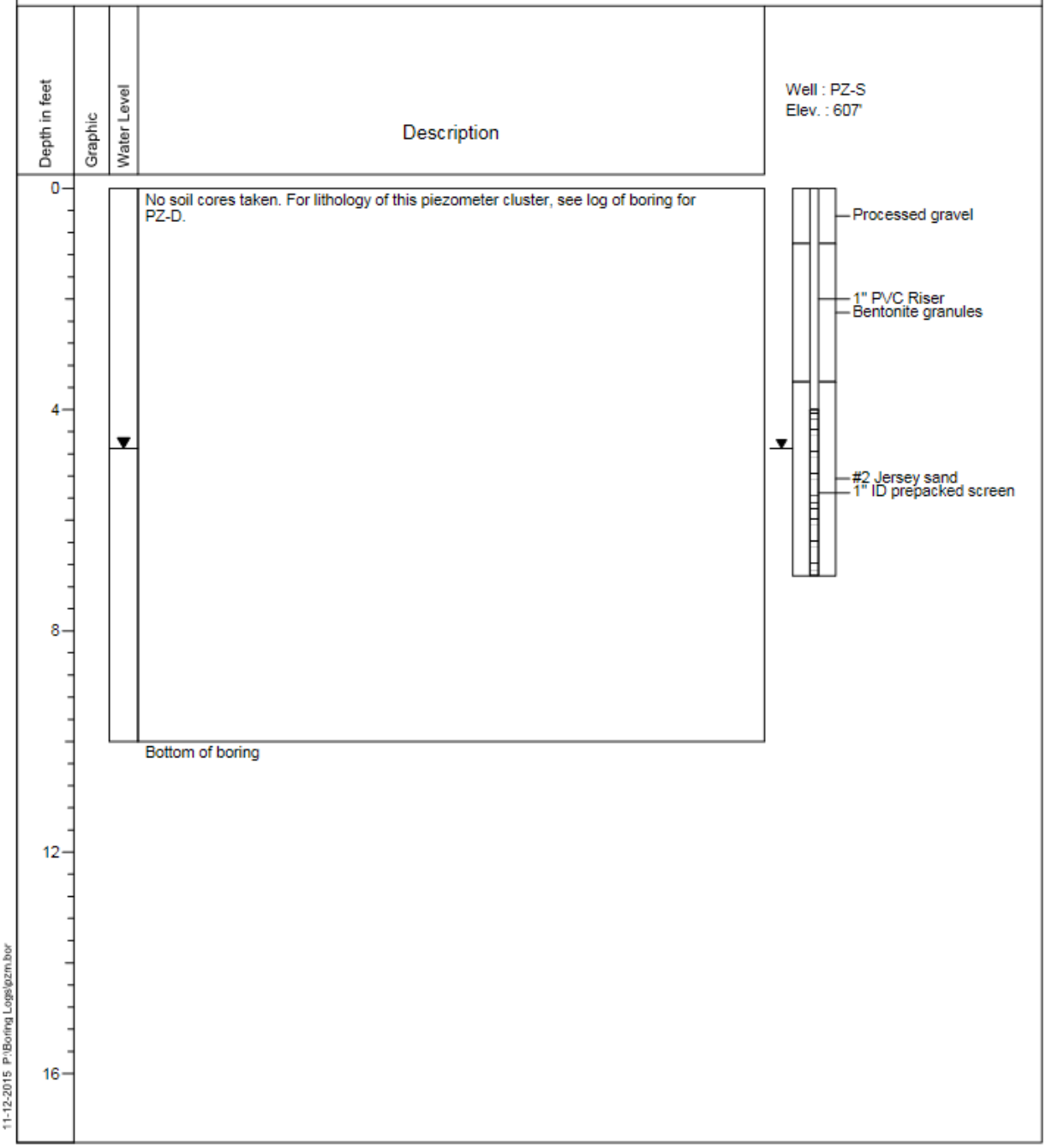

11-12-2015 P:\Boring Logs\pzm.bor

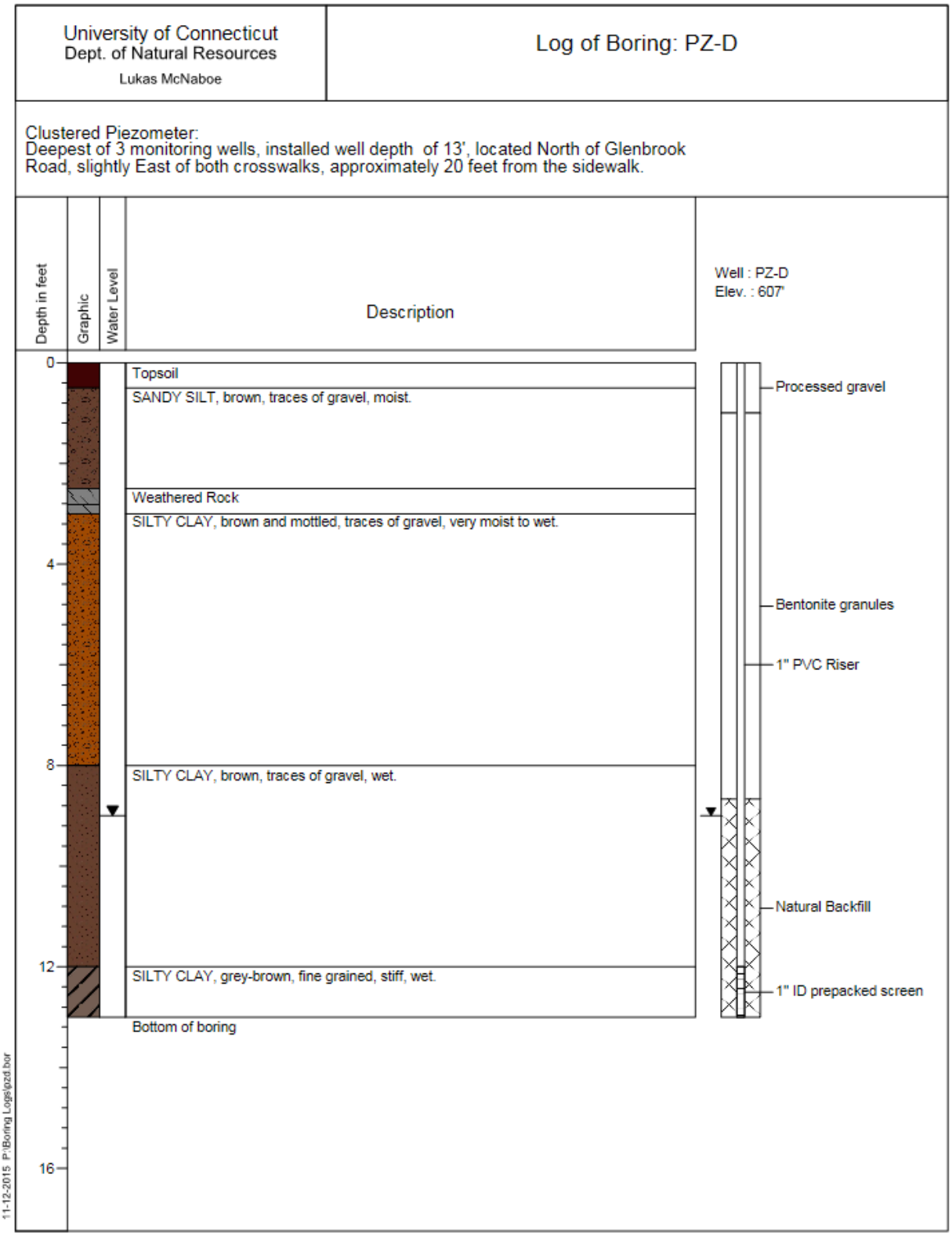
University of Connecticut
Dept. of Natural Resources
Lukas McNaboe
Log of Boring: PZ-D
Clustered Piezometer:
Deepest of 3 monitoring wells, installed well depth of 13', located North of Glenbrook Road, slightly East of both crosswalks, approximately 20 feet from the sidewalk.
Depth in feet
Graphic
Water Level
Description
Well : PZ-D
Elev. : 607'
0
4
8
12
16
Topsoil
SANDY SILT, brown, traces of gravel, moist.
Weathered Rock
SILTY CLAY, brown and mottled, traces of gravel, very moist to wet.
SILTY CLAY, brown, traces of gravel, wet.
SILTY CLAY, grey-brown, fine grained, stiff, wet.
Bottom of boring
Processed gravel
Bentonite granules
1" PVC Riser
Natural Backfill
1" ID prepacked screen
11-12-2015 P:\Boring Logs\pzd.bor

University of Connecticut
Dept. of Natural Resources
Lukas McNaboe

Log of Boring: PZ-D

Clustered Piezometer:
Deepest of 3 monitoring wells, installed well depth of 13', located North of Glenbrook Road, slightly East of both crosswalks, approximately 20 feet from the sidewalk.

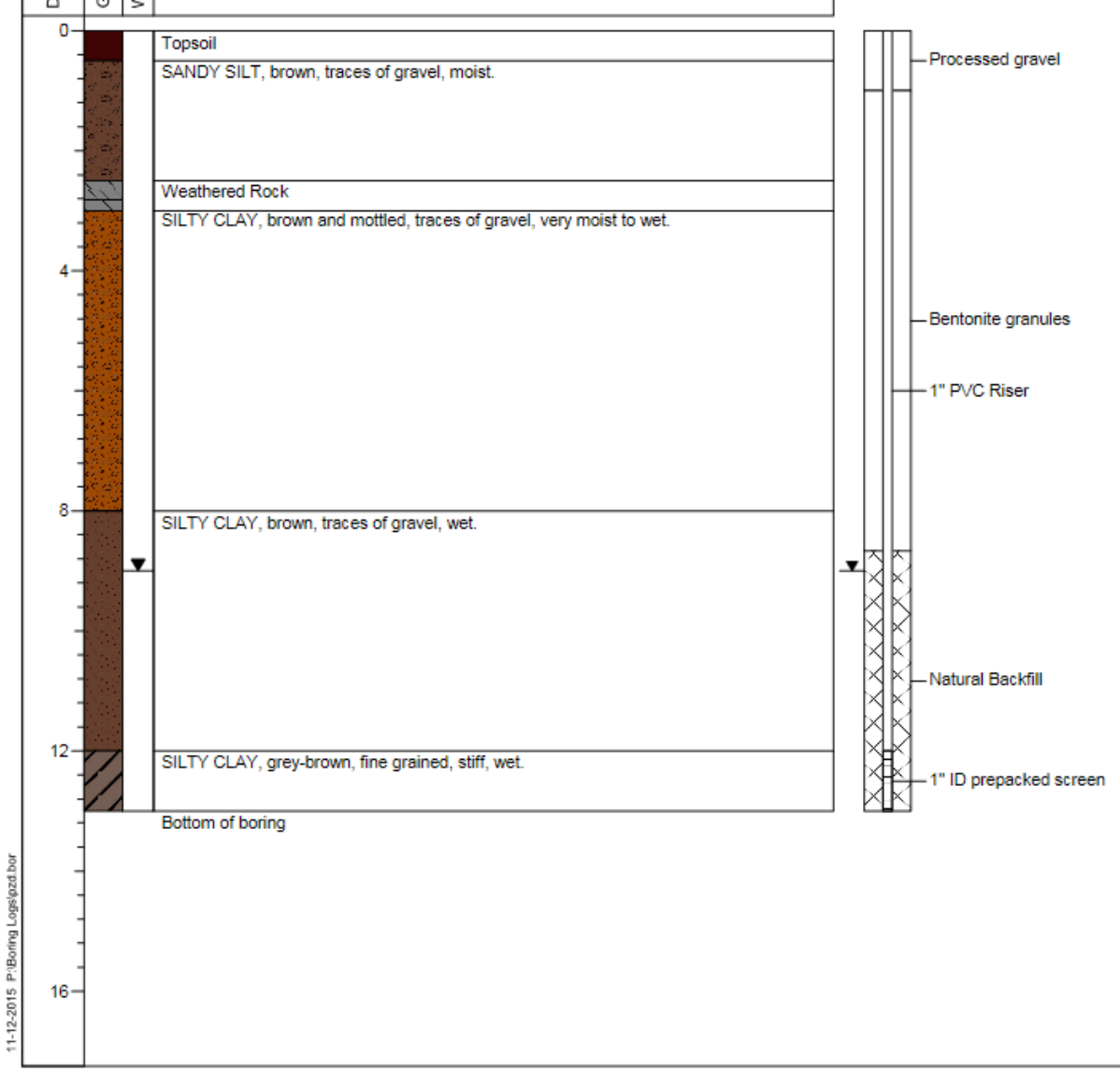

Appendix B

Equilibrium vapor-phase Rn calculations

Spreadsheet included in supplementary files.

Appendix C

Statistical analysis

The following information pertains to the mean separation test performed on the Cl^- data from the wells at the study site, as seen in Figures 2.19 and 2.20.

Distribution of Cl^- data:

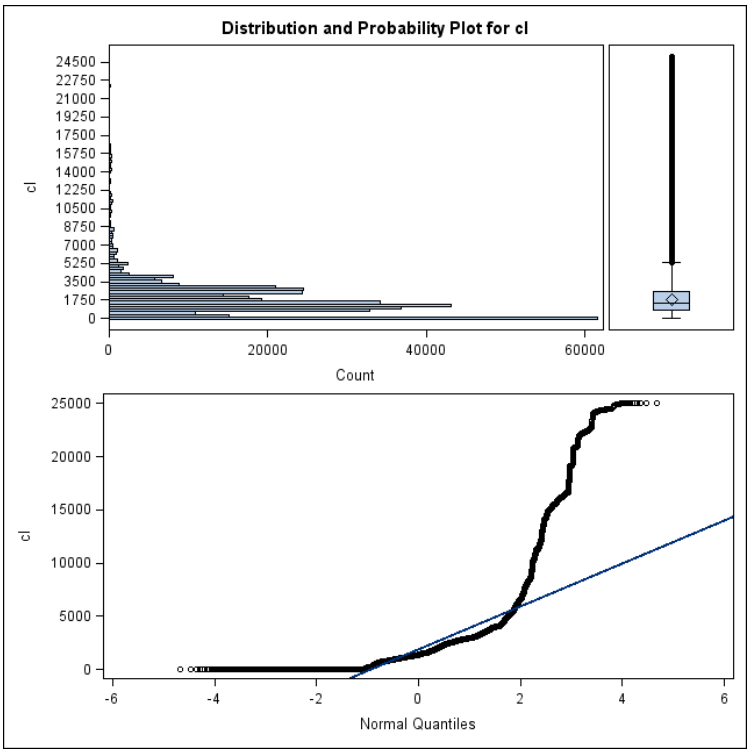

Distribution of Cl data

The UNIVARIATE Procedure
Variable: cl

Moments

N	407308	Sum Weights	407308
Mean	1839.92304	Sum Observations	749415374
Std Deviation	2023.09282	Variance	4092904.54
Skewness	4.08838621	Kurtosis	27.4593282
Uncorrected SS	3.04594E12	Corrected SS	1.66707E12
Coeff Variation	109.955295	Std Error Mean	3.16996405

Basic Statistical Measures

Location		Variability	
Mean	1839.923	Std Deviation	2023
Median	1398.673	Variance	4092905
Mode	0.000	Range	25042
		Interquartile Range	1804

Tests for Location: Mu0=0

Test	-Statistic-		-----p Value------	
Student's t	t	580.4239	Pr > |t|	<.0001
Sign	M	178246	Pr >= |M|	<.0001
Signed Rank	S	3.177E10	Pr >= |S|	<.0001

Tests for Normality

Test	--Statistic---		-----p Value------	
Kolmogorov-Smirnov	D	0.181554	Pr > D	<0.0100
Cramer-von Mises	W-Sq	3396.016	Pr > W-Sq	<0.0050
Anderson-Darling	A-Sq	21505.09	Pr > A-Sq	<0.0050

Distribution of log(Cl^-) data:

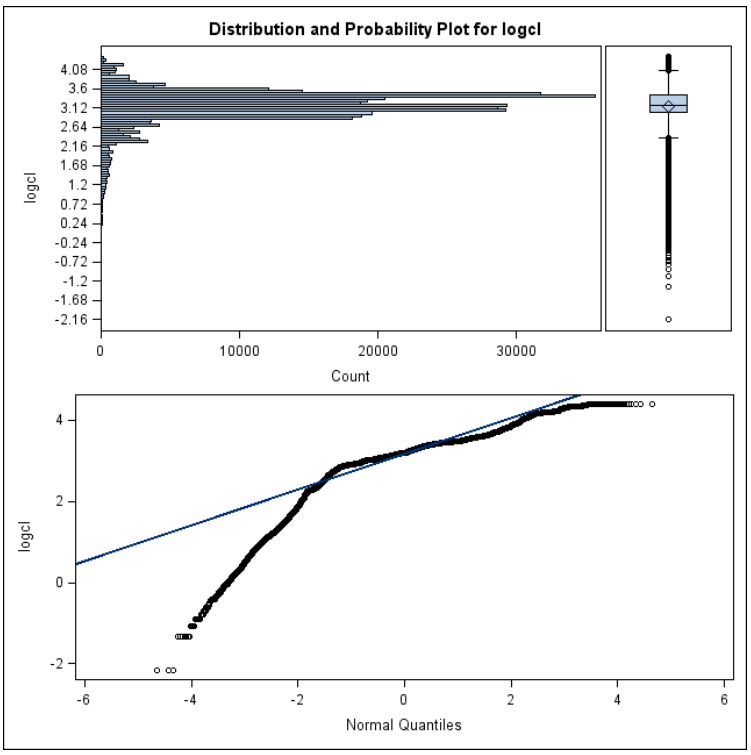

Distribution of log(Cl) data

The UNIVARIATE Procedure
Variable: logcl

Moments

N	356492	Sum Weights	356492
Mean	3.16445875	Sum Observations	1128104.23
Std Deviation	0.44227559	Variance	0.19560769
Skewness	-2.0120214	Kurtosis	8.62454279
Uncorrected SS	3639571.68	Corrected SS	69732.3825
Coeff Variation	13.9763423	Std Error Mean	0.00074074

Basic Statistical Measures

Location		Variability	
Mean	3.164459	Std Deviation	0.44228
Median	3.196451	Variance	0.19561
Mode	3.009345	Range	6.56488
		Interquartile Range	0.42395

Tests for Location: Mu0=0

Test	-Statistic-		-----p Value------	
Student's t	t	4272.001	Pr > |t|	<.0001
Sign	M	178084	Pr >= |M|	<.0001
Signed Rank	S	3.177E10	Pr >= |S|	<.0001

Tests for Normality

Test	--Statistic---		-----p Value------	
Kolmogorov-Smirnov	D	0.130145	Pr > D	<0.0100
Cramer-von Mises	W-Sq	1792.067	Pr > W-Sq	<0.0050
Anderson-Darling	A-Sq	11156.72	Pr > A-Sq	<0.0050

Since the log transformation improved the normality of the data (kurtosis and skewness coefficients closer to 3 and 0, respectively), this data set was used for the mean separation test between all wells, and the two-sample t-test between the upgradient well and all others.

Pertinent SAS output for mean separation test

Mean separation between all wells run

The GLIMMIX Procedure

Type III Tests of Fixed Effects

Effect	Num DF	Den DF	F Value	Pr > F
well	5	356E3	25982.7	<.0001

Significant differences exist between wells ($p<0.05$, H_0: no differences)

Mean separation between all wells run

The GLIMMIX Procedure

Tukey-Kramer Grouping for well Least Squares Means (Alpha=0.05)

LS-means with the same letter are not significantly different.

well	Estimate		*Antilog of LS Mean estimate (mg Cl^- L^{-1})*
UG1	3.3083	A	2033.8 – UG-1
PZS	3.2954	B	1974.2 – PZ-S
DG3	3.2795	C	1903.3 – DG-3
DG1	3.2118	D	1628.5 – DG-1
DG4	3.0120	E	1028.0 – DG-4
DG2	2.5920	F	390.8 – DG-2

Two sample T-test between up- and down-gradient wells 95259

The TTEST Procedure

Variable: logcl

Antilog of mean (mg Cl^- L^{-1})

loc	N	Mean	Std Dev	Std Err	Minimum	Maximum
DG	263317	3.1136	0.4773	0.000930	-2.1662	4.3987
UG	93175	3.3083	0.2769	0.000907	1.3013	3.8214
Diff (1-2)		-0.1947	0.4339	0.00165		

2033.8 – UG-1

1299.0 – DG wells

loc	Method	Mean	95% CL Mean		Std Dev	95% CL Std Dev	
DG		3.1136	3.1118	3.1154	0.4773	0.4760	0.4786
UG		3.3083	3.3065	3.3100	0.2769	0.2757	0.2782
Diff (1-2)	Pooled	-0.1947	-0.1979	-0.1914	0.4339	0.4329	0.4349
Diff (1-2)	Satterthwaite	-0.1947	-0.1972	-0.1921			

Method	Variances	DF	t Value	Pr > |t|
Pooled	Equal	356490	-117.70	<.0001
Satterthwaite	Unequal	281797	-149.84	<.0001

Mean Cl- concentrations are significantly different ($p<0.001$, reject H_0 of no differences)

Equality of Variances

Method	Num DF	Den DF	F Value	Pr > F
Folded F	263316	93174	2.97	<.0001

Due to the inequality of variances ($p<0.001$, H_0 equal variances), the Satterthwaite test should be used.

The following tables include the pertinent output relating to the statistical analysis of the regression lines in Figures 2.22 and 2.23. Statistical analysis was performed using SPSS software.

Na vs Ra – Figure 2.20

Variables Entered/Removed[a]

Model	Variables Entered	Variables Removed	Method
1	Na[b]	.	Enter

a. Dependent Variable: Ra

b. All requested variables entered.

Model Summary

Model	R	R Square	Adjusted R Square	Std. Error of the Estimate
1	.959[a]	.920	.908	1.92293

a. Predictors: (Constant), Na

ANOVA[a]

Model		Sum of Squares	df	Mean Square	F	Sig.
1	Regression	296.165	1	296.165	80.095	.000[b]
	Residual	25.884	7	3.698		
	Total	322.049	8			

a. Dependent Variable: Ra

b. Predictors: (Constant), Na

EC vs ln(Rn) – Figure 2.21

Variables Entered/Removed[a]

Model	Variables Entered	Variables Removed	Method
1	EC[b]	.	Enter

a. Dependent Variable: Ln_Rn

b. All requested variables entered.

Model Summary

Model	R	R Square	Adjusted R Square	Std. Error of the Estimate
1	.737[a]	.543	.451	.35448

a. Predictors: (Constant), EC

Coefficients[a]

Model		Unstandardized Coefficients		Standardized Coefficients	t	Sig.
		B	Std. Error	Beta		
1	(Constant)	6.606	.188		35.180	.000
	EC	-5.808E-005	.000	-.737	-2.437	.059

a. Dependent Variable: Ln_Rn

Appendix D

Chloride travel time calculations

Table D.1 Estimation of groundwater travel times between each well and its respective Cl^- recharge zone, as discussed in section 2.3.4.1. A K value of 2.63×10^{-4} cm s^{-1}, measured for this site in Angel (2015) was used for these approximations. Water level measurements taken on 3/3/2016 were used to calculate the hydraulic gradient. Porosity values of 0.3 and 0.6 were used to estimate the possible ranges of average groundwater velocity.

Well	**Peak time (months)**	**Distance traveled (m)**	**Comments**
UG-1	3	2.25-1.12	Second of 2 peaks
DG-1	0	0	Peak Cl^- coincides with peak de-icing
DG-2	4	2.99-1.50	
PZ-S	5	3.74-1.87	
DG-3	10	3.74-7.49	
DG-4			No clear peak observed